This is a preprint, the final version is subject to change, of the American Mineralogist (MSA)
Cite as Authors (Year) Title. American Mineralogist, in press.
(DOI will not work until issue is live.) DOI: http://dx.doi.org/10.2138/am-2016-5462

Revision 1

Zircon saturation and Zr diffusion in rhyolitic melts, and zircon growth geospeedometer

Youxue Zhang* and Zhengjiu Xu

Department of Earth and Environmental Sciences, the University of Michigan, Ann Arbor, MI 48109, USA

ABSTRACT

Zircon is a ubiquitous accessory mineral in silicic igneous rocks. We have carried out new zircon dissolution experiments to refine our understanding of Zr diffusion and zircon solubility in several rhyolitic melts. Zr diffusivity depends strongly on temperature and H_2O content, and weakly on pressure and anhydrous melt composition. The diffusion data for each individual melts follow the Arrhenius relation. The dependence of Zr diffusivity on temperature, pressure and melt composition (including H_2O content) is modeled for different rhyolitic melts in this study and for the combined literature and our data. Our data on Zr concentration at zircon saturation in silicic melts show strong dependence on temperature and weak dependence on pressure and melt composition, and are somewhat off the trend based on existing zircon solubility models. The dissolution or growth rate of a freely falling zircon crystal in a specific hydrous rhyolitic melt is modeled. The controlling factors are mostly the temperature and Zr concentration in the melt. Typical zircon growth rate in wet rhyolitic melt is 0.01 to 1.0 μm/yr. The size of zircon crystals can be used to place limit on the cooling rate of its hosting magma.

* Email: youxue@umich.edu

The presence of large indigenous zircon crystals in Bishop Tuff requires slow cooling of the Bishop Tuff magma chamber.

Keywords: Zirconium diffusion, Zr diffusivity, zircon solubility, zircon growth, zircon geospeedometer, cooling rate, Bishop Tuff

INTRODUCTION

Zircon is a common accessory mineral in continental rocks. Even though its abundance is low, it is one of the most often used minerals (e.g., Hanchar and Hoskin, 2003) in dating and in inferring paleo-formation conditions (Valley et al., 2005). Survival of pre-eruptive zircon crystals has often been reported, and these crystals can be used to obtain eruption history and magma chamber residence time (Simon et al., 2008). The formation and survival of zircon depends on the saturation condition (or solubility) of zircon and diffusivity of Zr in silicate melts, which have been investigated extensively (e.g., Watson, 1979; Watson and Harrison, 1983; Harrison and Watson, 1983; Ellison and Hess, 1986; Baker and Watson, 1988; Keppler, 1993; LaTourrette et al., 1996; Mungall et al., 1999; Koepke and Behrens, 2001; Baker et al., 2002; Hanchar and Watson, 2003; Rubatto and Hermann, 2007; Behrens and Hahn, 2009; Boehnke et al., 2013).

Still there are unresolved issues. One is the dependence of Zr diffusivity on melt composition, especially the H_2O content. In the earlier years, it was not easy to directly measure H_2O concentrations in experiments, but now with FTIR it is straightforward to determine H_2O concentrations in experimental charges. Natural silicate melts span a large compositional range.

We limit our experimental study to different rhyolitic melts because zircon forms and survives more easily in rhyolitic melts (Boehnke et al., 2013). However, in modeling, we try to combine with previous data so as to cover a large range of melts from basalts to rhyolites. The second is the dependence of Zr diffusion and zircon solubility on pressure. Although crustal pressure variation is not large, nonetheless it is of interest to understand the pressure effect for accurate prediction of these properties. We aim at obtaining the dependence of Zr diffusivity as a function of temperature, pressure, melt composition and water content. We also compare our zircon solubility data with the recent model by Boehnke et al. (2013). Furthermore, we will use the data to evaluate zircon dissolution kinetics as part of our systematic studies of mineral dissolution kinetics in silicate melts (Zhang and Xu, 2003; Chen and Zhang, 2008, 2009). Finally, we explore the use of newly grown zircon crystal size to constrain host magma cooling rates.

EXPERIMENTAL AND ANALYTICAL METHODS

Zircon dissolution experiments are conducted in piston-cylinder apparatus to investigate Zr diffusion and zircon solubility in dry and hydrous rhyolitic melts at 0.5 to 1.5 GPa and 1270-1890 K. ZrO_2 concentration profiles are measured by electron microprobe. Experimental and analytical methods mostly follow those of Harrison and Watson (1983) and Zhang et al. (1989), and details can be found below.

Starting materials

The starting materials include a large zircon crystal and five rhyolitic glasses. The large transparent gem-quality zircon crystal was purchased online and measures 13 mm × 8 mm × 7 mm. The composition of this zircon crystal is roughly $Hf_{0.013}Zr_{0.987}SiO_4$ (Table 1). After cutting, the best zircon wafers without visible cracks and inclusions under microscope are chosen for experiments. Starting rhyolitic glasses include three natural glasses in our collection: Newberry Crater obsidian with about 0.1 wt% total H_2O (Newman et al., 1986), CIT-1 with 0.2 wt% total H_2O (Newman et al., 1986), and bb3b-7b from Mono Craters (Sieh and Bursik, 1986; Newman et al., 1988) with 1.1 wt% H_2O. In order to examine the effect of H_2O on Zr diffusion, two hydrous rhyolitic glasses synthesized in our earlier studies (Liu et al., 2005; Hui et al., 2008, 2009) were used: one contains about 5.5 wt% H_2O, and the other contains about 3.6 wt% H_2O. Chemical compositions of the rhyolitic glasses on dry basis are listed in Table 1. The total H_2O contents measured on glass chips before experiments by FTIR are also listed. H_2O concentrations on selected experiments are also measured after experiments and these are reported with experimental conditions later (Table 2). For easy referencing, the rhyolitic glass samples are renamed Rhy1 (Newberry Crater obsidian), Rhy2 (synthesized hydrous rhyolitic glass containing 3.6 wt% H_2O), Rhy3 (Mono Crater obsidian bb3b-7b), Rhy4 (CIT-1), and Rhy5 (synthesized hydrous rhyolitic glass containing about 5.5 wt% H_2O) by increasing SiO_2+Al_2O_3 concentration or increasing viscosity on the dry melt basis. The SiO_2+Al_2O_3 concentration varies from 86.9 to 89.9 wt%, and the cation ratio M (=(Na+K+2Ca)/(Al·Si)) defined by Watson and Harrison (1983) to quantify the dependence of zircon solubility on composition varies from 1.36 to 1.54. The calculated "dry" melt viscosity at 1500 K is also listed, which shows that the small compositional variation has significant effect on viscosity and hence presumably on Zr diffusivity (e.g., Mungall, 2002). For comparison, compositions of Lake County obsidian (LCO)

used by Harrison and Watson (1983) and Baker et al. (2002), and of haplogranite8 (HPG8) used by Mungall et al. (1999) in studying Zr diffusion are also listed in Table 1 (last two columns).

Experiments

Zircon dissolution experiments were carried out in end-loaded piston-cylinder apparatus with a piston diameter of 12.7 mm at the University of Michigan following the procedures of Chen and Zhang (2008, 2009). The starting rhyolitic glass is prepared into a cylinder of 1.6 to 2.6 mm diameter and about 1.2 to 1.9 mm thickness. The starting zircon crystal is prepared into a cylinder of the same diameter as the glass and about 1.0 to 1.9 mm thickness. One base of the glass and the zircon crystal is polished. The glass and zircon crystal are loaded into a capsule as a cylinder stack with the zircon wafer in the bottom and the rhyolitic glass wafer on the top and the polished bases as interface between them. This configuration ensures gravitational stability to minimize convection because dissolved zircon component is expected to have a higher density than the rhyolitic melt. The capsule material is graphite for anhydrous rhyolite (0.1 to 0.2 wt% H_2O), Au75Pd25 for hydrous rhyolite at experimental temperature < 1500 K, and Pt for hydrous rhyolite at ≥1500 K. The capsule is then fitted into the usual piston-cylinder assembly (see figure 1 in Ni et al., 2009b), including MgO sleeves, graphite heater, and $BaCO_3$+toner pressure medium. Care is taken so that the contact interface of zircon and glass is at the center of the furnace so that the temperature maximum will be at the sample interface during the experiment.

Once placed into the piston-cylinder apparatus with end-loaded pressure applied and electric cables and cooling water connected, the pressure is slowly increased to the desired pressure using a piston-out procedure. Then the sample is heated to 473 K and maintained there typically overnight for relaxation of the assemblage. Then, the temperature is rapidly heated to

the intended temperature and maintained there for the planned duration. Quench is achieved by turning off the power to the furnace, with typical cooling rate of 100 K/s based on actual recording.

The complete temperature history is recorded, allowing the detection of rare sudden temperature variation, which can be useful to understand unexpected experimental results. Fig. 1 displays the recorded temperature history for two experiments (ZirDis1 and ZirDis2), which shows that the temperature fluctuation is minimal for experiment ZirDis1, but the temperature dropped suddenly by 670 K at ~30 minutes before quenching due to some event or thermocouple failure (when no experimentalist was manually monitoring the experiment). Such observations are useful when interpreting experimental results.

A 6% correction to the nominal pressure is applied based on pressure calibration (Hui et al., 2008; Ni and Zhang, 2008). Effort was made so that the zircon-glass interface was at the center of the furnace. Because the thermocouple tip that recorded the experimental temperature is not at the sample center, a correction to the recorded temperature is made to obtain the temperature at the zircon-melt interface using the temperature calibration of Hui et al. (2008). Because the half thickness of glass+zircon is less than 2 mm, and especially the diffusion profile is typically less than 0.5 mm, the temperature difference across the charge inside the capsule is $\leq$ 5 K according to the calibration of Hui et al. (2008). However, the actual temperature uncertainty and gradient may be larger because the interface position may not be perfectly aligned with the hottest spot during an experiment, although effort was made to make it so.

After quench, the experimental charge is taken out of the pressure medium and embedded in epoxy, ground to roughly the mid-section (widest section), and polished on one side for electron microprobe analyses of ZrO_2 concentration. To check for possible water loss during the

experiments, selected experimental charges using hydrous rhyolitic glasses are polished on both sides for FTIR analyses of H_2O. Experimental conditions are listed in Table 2.

Electron microprobe analyses

Major oxide concentrations of zircon and glasses are measured before and after experiments using Cameca SX100 electron microprobe at the University of Michigan's Electron Microbeam Analysis Laboratory (EMAL). ZrO_2 concentration profiles in rhyolite glass as a function of distance away from the zircon-glass interface are also measured using the electron microprobe but in a separate procedure.

For analyses of zircon pieces, concentrations of SiO_2, ZrO_2, HfO_2, TiO_2, Al_2O_5, FeO, P_2O_5, ThO_2, and UO_2 are measured, but only SiO_2, ZrO_2 and HfO_2 concentrations are significantly above the detection limit. Analysis conditions include an acceleration voltage of 15 kV and beam current of 20 nA. Utu-zircon is used as the standard for SiO_2, ZrO_2 and HfO_2 analyses. The average concentrations of the three oxides are reported in Table 1.

For major oxides in obsidian glasses, the normal rhyolitic glass analysis procedure that we often use (e.g., Zhang et al., 1997; Ni and Zhang, 2008) is used to analyze SiO_2, TiO_2, Al_2O_2, FeO(total), MgO, CaO, Na_2O and K_2O. Analysis conditions are: 15 kV, 2 nA current for hydrous samples and 5 nA for anhydrous samples, and 5 μm beam diameter. To circumvent Na loss, Na_2O concentration is based on 5 counting periods each lasting 4 s, and extrapolation to zero time. The averaged data are reported in Table 1.

A separate special procedure is made to measure only ZrO_2 in glass as a function of distance away from the zircon-glass interface. For matrix correction, the major oxide concentrations are taken from the averages of earlier separate major oxide measurements.

Analysis conditions are: Lα line of Zr, 15 kV, 40 nA current (to improve the detection limit), point beam or, for longer profiles, 5 μm by 5 μm raster mode, and using all 4 crystals to count Zr-Lα line for 240 s. Both Utu-zircon and our own zircon crystal (that is used for dissolution experiments) are used as the standard for ZrO_2.

The accuracy (the closeness of the microprobe analyses to the true concentrations) and precision (the reproducibility of the microprobe analyses) of the microprobe analyses of ZrO_2 in glasses can be gauged from the analyses of ZrO_2 in the far-field of 7 experiments using Rhy1 as the starting glass. Rhy1 contains 454±1 ppm ZrO_2 based on 3 analyses by XRF and ICP-MS. Ninety-seven electron microprobe analyses of this sample in the far-field gave 499±57 ppm (e.g., Fig. 2). Hence, the accuracy (or offset) based on 97 analyses is about 45 ppm ZrO_2 (0.0045 wt%) and the 1σ precision is 57 ppm ZrO_2 (0.0057 wt%), which are small compared to the ZrO_2 concentration levels in most experiments. The detection limit for ZrO_2 (using 2σ) is about 114 ppm. Note that the accuracy does not affect the determination of Zr diffusivity.

Measurements of ZrO_2 concentration near zircon may contain signals from secondary fluorescence, which would produce an apparent ZrO_2 concentration profile near zircon (Harrison and Watson, 1983; Zhao et al., 2015). In order to quantify the secondary fluorescence, we prepared a couple with zircon crystal and rhyolite glass (Rhy1) in good contact at polished surfaces, and used the same microprobe procedure to measure ZrO_2 concentration profile in the glass. The results are shown in Fig. 2. It can be seen that near the interface (within about 10 μm), the secondary fluorescence produces an apparent increase in ZrO_2 concentration, which was fit as $0.0518e^{-x/3.374}$ where 0.0518 is in wt% and x is distance from the zircon-glass interface in μm. This apparent extra ZrO_2 has been subtracted from all ZrO_2 diffusion profiles reported below.

Accurate measurement of distance away from the zircon-glass interface is very important for accurate retrieval of the diffusivity, especially for short profiles. Because the microbeam position may shift during microprobe analyses, we used a couple of methods to ensure that the measured distance is accurate. (1) To determine the interface position accurately, each traverse runs from inside zircon to the glass. This way, one point is often close enough to the interface with ZrO_2 concentration between that in ZrO_2 (66.38 wt%) and that in the melt (typically < 1 wt%). If the concentration is about the average of the two concentrations, then the point is centered at the interface and the distance to the interface is defined to be zero. If it is higher or lower than the average, the distance can be estimated from the fraction of each phase needed to produce the measured concentration. In this way, the interface position relative to the measured points can be estimated to an accuracy of better than 0.5 μm. (2) After the electron microprobe analyses, the analyzed spots can be seen under optical microscope. We verified the distance between each spot and the zircon-glass interface using an optical microscope for points within 50 μm of the interface. (3) If the measured concentration profile is not perpendicular to the interface, we used the distance of the point to the interface rather than the traverse distance, either by optical measurement, or by calculation as the apparent distance multiplied by $\sin\theta$ where θ is the angle between the profile and the interface. (4) We typically measure three or more traverses in the same charge. If there are many cracks, more traverses are measured. One purpose of measuring different traverses is to make sure that diffusion is one-dimensional and without convection. The second purpose is to compare the different traverses to estimate the true distance gap across a crack.

Fourier transform infrared spectroscopy

To check for possible water loss during experimental heating, and because different pieces of glass from the same synthesis or from the same hand specimen can be slightly inhomogeneous in H_2O concentration, total H_2O concentrations of hydrous glasses after experiments are measured following the procedures in our earlier publications (e.g., Zhang et al., 1997; Liu and Zhang, 2000; Xu and Zhang, 2002; Ni et al., 2008). Only a brief summary of the procedures is provided here. After electron microprobe analyses, the experimental charge is doubly polished to about 0.6 to 1.0 mm thickness. The thickness of the sample is measured using a digital micrometer. Then the sample is analyzed using the infrared microscope attachment (AutoImage) of Perkin-Elmer Spectrum GX FTIR spectrometer at the University of Michigan, with a NIR source, a CaF_2 beamsplitter, and a liquid-N_2-cooled MCT detector. Molar absorptivities of Newman et al. (1986) and Dobson et al. (1989) are used to calculate the total H_2O concentration. The data are reported in Table 2.

RESULTS

The experimental charges are crack-free when a metal capsule (Au75Pd25 or Pt) is used, but often contain cracks when graphite capsule is used. If avoiding cracks is critical, then metal capsules are the best when iron loss is not a major issue. Figure 3 shows a BSE image (left-hand side) of an experimental charge and a photomicrograph of another charge with different scales, one with cracks (graphite capsule) and the other without cracks (Au75Pt25 metal capsule). When electron microprobe traverses are taken, effort is made to avoid cracks or pits.

Water concentrations measured for selected experimental charges show that water concentration is not significantly different from the initial concentration. Hence, loss of water is ignored in the treatment below.

Convection is deemed to be insignificant because the melt is on top of the zircon crystal, viscosity of rhyolitic melt is high, the diffusion profile length is short (< 0.2 mm), and several traverses measured in the same experimental charge are in good agreement (Figs. 4 and 5).

The ZrO_2 concentration profiles in the melt near the interface measured by electron microprobe need special care. One effect is that very close to the interface (0-1 μm), the beam samples zircon crystal itself, causing high ZrO_2 concentration (higher than the true interface melt concentration). The second effect is secondary fluorescence discussed earlier. The third is due to growth of zircon during quench (Zhang et al., 1989; Yi et al., 2015), which depletes ZrO_2 near the interface in a 1-6 μm thick layer, depending on the experimental temperature since the quench rate is roughly fixed). The depletion due to quench growth is not part of the diffusion profile during zircon dissolution. Hence, this part of the profile is not included in fitting of the profile to obtain Zr diffusivity and zircon solubility. Furthermore, when a crack is crossed in a traverse, other traverses are used to estimate the true distance across the crack. Using these steps, the composite concentration profiles based on several traverses are smooth with only very small scatter similar to the analytical precision, ±0.006 wt% ZrO_2 absolute (1σ) or 1% relative (Figs. 4 and 5). The high-quality data allow us to retrieve diffusivity and interface melt composition with high reliability.

Some experimental and analytical issues

Some experiments and data showed complexity and are discussed below:

1. Two experimental samples (ZirDis8 at 1357 K, the lowest-temperature experiment on Rhy1 at 0.5 GPa, and ZirDis17 at 1483 K, the lowest-temperature experiment on Rhy1 at 1.5 GPa) partially crystallized, with degree of crystallization ≥ 20%. The crystallization is due to the low temperatures of the two experiments. When analyzing ZrO_2 concentrations, each point was manually chosen so that it was in the glassy region away from crystals. Even though the concentration profiles appear smooth and can be fit well, the diffusivity and solubility values obtained are off the trend defined by other data. Hence, they are not used.

2. The results of ZirDis9 using melt composition Rhy4 seem to be outliers in plots. Hence, a repeated experiment, ZirDis19, at the same temperature and pressure using the same melt is carried out. Zr diffusivity and interface ZrO_2 concentration obtained from ZirDis19 are both significantly lower than those in ZirDis9, but the mid-concentration distance (Zhang, 2008, p. 45) is only about 5 μm, too short for accurate diffusivity determination (Ganguly et al., 1988). Because these 2 experiments are the only experiments on Rhy4, results from both experiments are not used in later fitting. The likely source of error is misalignment of the zircon-melt interface with the hotspot of the heater, resulting in large temperature errors.

3. Experiment ZirDis2 experienced a sudden temperature drop (Fig. 1), during which the zircon crystal must have grown, and the concentration profile for ZirDis2 shows that ZrO_2 concentrations within a 40 μm distance from the interface are lower than expected from the trend (Fig. 4). The fitting excluded data in the 40-μm thick layer (Fig. 4). The length of the affected profile suggests that the temperature did not recover after the drop although the recording indicates the opposite. Initially we thought that the data should be discarded. However, a repeated experiment at similar conditions (ZirDis4) provided similar Zr diffusivity and interface ZrO_2 concentration. Hence, the results of ZirDis2 are retained in the data treatment and figures.

4. There is small horizontal heterogeneity in Experiment ZirDis14: the different traverses do not overlap within analytical uncertainty (Fig. 5). The effect is deemed small and tolerable, and the results are still used.

5. The large scatter in the concentration profiles of ZirDis6b at 1270 K is due to the low overall ZrO_2 concentration of 0.01 to 0.08 wt%, and the 1σ analytical error of 0.0057 wt% ZrO_2 (or 2σ of 0.0114 wt% ZrO_2) is significant compared to the concentration. Because this experiment provides important constraint on Zr diffusivity and zircon solubility at low temperature, the data are kept.

Fitting ZrO_2 concentration profiles

The combined profile of each experiment is fit to provide ZrO_2 diffusivity and ZrO_2 concentration in the interface melt, which is assumed to be the saturation concentration of ZrO_2 in the melt in equilibrium with zircon (Harrison and Watson, 1983). The profiles are fit by the following equation (Zhang et al., 1989, Zhang, 2008):

$$C = C_\infty + (C_0 - C_\infty)\frac{\mathrm{erfc}(\frac{x}{\sqrt{4Dt}} - a)}{\mathrm{erfc}(-a)}, \quad (1)$$

where C is measured ZrO_2 concentration at each point of x (distance away from the interface), C_∞ is the initial ZrO_2 concentration in the melt, C_0 is ZrO_2 concentration in the interface melt as a fitting parameter, t is experimental duration, and D is Zr diffusivity as a fitting parameter, and the parameter a is solved from (Zhang et al., 1989, Zhang, 2008):

$$\sqrt{\pi} a e^{a^2} \mathrm{erfc}(-a) = \frac{C_0 - C_\infty}{C_c - C_0}, \quad (2)$$

where C_c is ZrO_2 concentration in zircon (66.38 wt%, Table 1). There are two fitting parameters in eq. (1), C_0 and D. C_∞ is measured by averaging the many points of the far-field melt composition, and a is calculated from eq. (2) in which C_c is known (Table 1). The fitting is carried out iteratively. First, a C_0 value is estimated by eyeballing of the concentration profile, and the parameter a is solved from eq. (2). Using this a value, the concentration profile is fit by eq. (1), from which C_0 value is obtained. Using the new C_0 value, a is solved again from eq. (2), and another fit is carried out. This procedure is repeated until the C_0 value does not change any more. The fits are shown as curves in Figs. 4 and 5. The quality of the fits assuming constant D_{Zr} is excellent, even when the total ZrO_2 concentration is large from 0 to 5.2 wt% (ZirDis1), and total SiO_2 concentration variation across a profile is about 3.6 wt%. Note that the value of the parameter a is close to zero (≤ 0.045), meaning that even if it is taken to be zero, not much error would be introduced in eq. (1).

Zr diffusivity and the ZrO_2 concentration in the interface melt obtained from the fitting are reported in Table 2. Fitting errors are also reported. The 1σ errors are small, 0.3-5% relative for the interface ZrO_2 concentration, and 0.9-12% relative for Zr diffusivity. Most of the experimental uncertainty is likely in the temperature due to small misalignment of the interface with the hotspot, which cannot be quantified.

Because the zircon crystal contains 1.3 mol% of $HfSiO_4$, assuming ideal solution for the $ZrSiO_4$ component in zircon, the saturation ZrO_2 concentration of pure $ZrSiO_4$ zircon is the reported C_0 value divided by 0.987. We will use C_0 to denote the extrapolated interface ZrO_2 concentration, and C_{sat} to denote the saturation ZrO_2 concentration in equilibrium with pure zircon, where $C_{sat} = C_0/0.987$.

Zircon dissolution distance

Zircon dissolution distance is typically less than 1 μm and cannot be measured directly using optically. By measuring ZrO_2 concentration profiles away from zircon, extra ZrO_2 mass in the glass (melt) can be evaluated by integration, and the dissolution distance can be estimated using the following equation (Zhang et al., 1989) when variation of melt density with distance x can be ignored:

$$L_c = \frac{\rho_m}{\rho_c} \frac{1}{(C_c - C_\infty)} \int_0^\infty (C - C_\infty) \mathrm{d}x , \quad (3a)$$

where L_c is the crystal dissolution distance, ρ_m is glass density (since the concentration measurement is made in quenched glass) at room temperature assumed to be a constant in each experiment (calculated using the rhyolitic glass density as a function of H_2O concentration, Zhang, 1999), ρ_c is crystal density (4669 kg/m^3, Robie and Hemingway, 1995), C_c is ZrO_2 concentration in the crystal, C_∞ is ZrO_2 concentration in the initial melt, and C is ZrO_2 concentration at any point x. Using eqs. (1) and (2), eq. (3a) can be integrated to obtain:

$$L_c = \frac{\rho_m}{\rho_c} a\sqrt{4Dt} . \quad (3b)$$

The dissolution distance L_c so calculated is reported in Table 2. If one is interested in finding the melt growth distance L_m, it is $L_c(\rho_c/\rho_m)$, or about 2 times L_c.

Zr diffusivity in individual melts

Obtained Zr diffusion data from this study are shown in Fig. 6a. In each individual melt, the data follow the Arrhenius relation well (Fig. 6a). For Rhy1 (containing about 0.12 wt% H_2O)

at 1467-1885 K and 0.5 GPa, the four data points on Zr diffusivity can be fit by the following relation:

$$\ln D_{Zr} = -(11.561\pm1.988) - (32672\pm3303)/T, \quad r^2 = 0.980 \qquad (4a)$$

where T is in K, D_{Zr} is in m^2/s, and error bars on the fitting parameters are given at 1σ level hereafter. The activation energy is 272±27 kJ/mol, which is significantly smaller than 409±12 kJ/mol on a dry and more silicic melt (last column in Table 1) obtained by Harrison and Watson (1983), and also smaller than 353±27 kJ/mol for a dry and even more silicic melt (HPG8) obtained by Mungall et al. (1999). The largest error of eq. (4a) in reproducing experimental ln$D$ is 0.44, typical of diffusion studies.

Zr diffusivity in dry melts Rhy1 shows systematic variation with temperature and pressure. The diffusion data in Rhy1 (0.12 wt% H_2O) at 0.5 to 1.5 GPa (7 points) can be described well by the following equation:

$$\ln D_{Zr} = -(13.270\pm2.137) - [(30747\pm3504) - (1856\pm585)P]/T, \quad r^2 = 0.980 \qquad (4b)$$

where D is in m^2/s, P is in GPa, and T is in K. The maximum error of the above equation in reproducing experimental ln$D$ values is 0.53. When the pressure increases by 1 GPa, lnD_{Zr} increases by about 1.0, a measurable but not huge effect. The increase of D_{Zr} with pressure indicates a negative activation volume for diffusion in this polymerized melt, which is consistent with a typically observed viscosity decrease with pressure in polymerized melts (e.g., Kushiro, 1980).

For Rhy5 (containing about 5.5 wt% H_2O) at 0.5 GPa, the Arrhenius relation for three data points of Zr diffusivity is:

$$\ln D_{Zr} = -(12.391\pm0.305) - (23639\pm441)/T, \quad r^2 = 0.9997 \qquad (4c)$$

The activation energy is 197±4 kJ/mol, which is similar to 198±8 kJ/mol for a similar melt composition (LCO) containing 6.0 wt% H_2O (Harrison and Watson, 1983). The largest error of eq. (4c) in reproducing the experimental ln$D$ is 0.05, excellent but there are only 3 points. Compared to Rhy1 (0.12 wt% H_2O), Zr diffusivity in Rhy5 (5.5 wt% H_2O) is higher by about 5 ln$D$ units at 1550 K. Because Zr diffusivity in dry Rhy5 is expected to be somewhat lower than that in dry Rhy1, the H_2O effect is slightly larger than 5 ln$D$ units per 5.5 wt% H_2O, e.g., ≥1 ln$D$ units per wt% H_2O.

For Rhy2 (containing about 3.6 wt% H_2O) at 0.5 GPa, the three data points on Zr diffusivity can be expressed as:

$$\ln D_{Zr} = -(17.176\pm0.457) - (17964\pm681)/T, \quad r^2 = 0.9986 \qquad (4d)$$

The activation energy is 149±6 kJ/mol. The largest error in reproducing the experimental ln$D$ is 0.05. This activation energy seems too low for this melt containing intermediate amount of H_2O, and is significantly smaller than 197 kJ/mol for a hydrous HPG8 containing 3.7 wt% H2O from a two-point fit by Mungall et al. (1999). On the other hand, Baker et al. (2002) reported activation energies of 140±34 kJ/mol and 142±42 kJ/mol respectively for LCO containing 4.4 wt% and 1.7 wt% H_2O.

For Rhy3 (containing about 1.1 wt% H_2O), there are only two points. A linear fit is nonetheless carried out:

$$\ln D_{Zr} = -12.0 - 30360/T. \qquad (4e)$$

The activation energy is about 252 kJ/mol, which is only slightly lower than that for the dry melt and consistent with expectation. The error on the fitting parameters cannot be constrained because the straight line is drawn through only two points. Compared to dry Rhy1 (0.12 wt% H_2O), Zr diffusivity in Rhy3 (1.1 wt% H_2O) is higher by about 1 ln$D$ unit at 1550 K.

Zircon solubility in individual melts

The interface ZrO_2 concentration in the melt is shown in Fig. 6b. The saturation concentration is treated as due to equilibrium for the reaction

$$ZrSiO_4(\text{zircon}) = ZrO_2(\text{melt}) + SiO_2(\text{melt}). \quad (5)$$

Hence, it varies with temperature following the van't Hoff equation in each melt, and the data in Fig. 6b are consistent with this expectation.

In Rhy1 (with 0.12 wt% H_2O and $M = 1.54$) at 0.5 GPa, the saturation ZrO_2 concentration can be expressed as follows:

$$\ln C_{sat} = (10.609 \pm 0.901) - (17125 \pm 1498)/T, \quad r^2 = 0.9849 \quad (6a)$$

where T is in K and C_{sat} (= C_0/0.987) is the saturation ZrO_2 concentration in wt% (for 1 wt% ZrO_2, $C_{sat} = 1$). C_{sat} is interpreted to be ZrO_2 concentration in the melt at pure zircon saturation. The largest error in reproducing the experimental $\ln C_{sat}$ is 0.13. The standard state enthalpy for zircon dissolution is obtained from $8.314 \times (17.125 \pm 1.498) = 142 \pm 12$ kJ/mol, which is significantly higher than 84.0±0.3 kJ/mol by Boehnke et al. (2013). Rhy1 is a natural obsidian from Newberry Crater containing 0.0454 wt% ZrO_2. Using eq. (6a), the zircon saturation temperature in this melt is 1250 K (977°C), meaning that Newberry Crater obsidian erupted at a fairly high temperature for a rhyolite.

There is small but resolvable pressure effect in the solubility of zircon in dry Rhy1 from 0.5 to 1.5 GPa (Fig. 7). When pressure increases by 1 GPa, the ZrO_2 concentration at zircon saturation decreases, or zircon solubility decreases by 20-37%. Hence the pressure effect is to increase Zr diffusivity but to decrease zircon solubility. This pressure effect on solubility is expected because as pressure increases, the crystalline phase normally becomes more stable

compared to the melt due to the smaller partial molar volume of the $ZrSiO_4$ component in zircon than in the melt, leading to smaller solubility in the melt (or higher crystallization temperature of zircon from the melt). The saturation ZrO_2 concentration (wt%) for zircon in Rhy1 at 0.5 to 1.5 GPa (8 points) can be described well by the following equation:

$$\ln C_{sat} = (10.580\pm0.564) - [(16755\pm925) + (657\pm155)P]/T, \quad r^2 = 0.9940, \qquad (6b)$$

where P is in GPa, and T is in K. The above equation is able to reproduce experimental $\ln C_{sat}$ values for Rhy1 to within 0.13 $\ln C_{sat}$ units. ZrO_2 concentration at zircon saturation decreases by about 0.4 $\ln C_{sat}$ units when pressure increases by 1 GPa. The standard state reaction enthalpy is 142±8 kJ/mol (in agreement with eq. (6a) but with a better constrained error) at 0.5 and 148±11 kJ/mol at 1.5 GPa. The pressure effect means that a melt that is saturated with zircon at depth would become undersaturated with zircon upon ascending, leading to decompression induced zircon dissolution.

For Rhy5 (with 5.5 wt% H_2O and $M = 1.28$) at 0.5 GPa, the saturation ZrO_2 (wt%) depends on temperature as follows:

$$\ln C_{sat} = (10.604\pm1.082) - (16704\pm1563)/T, \quad r^2 = 0.9913 \qquad (6c)$$

The standard state reaction enthalpy is 139±13 kJ/mol, similar to that in dry rhyolitic melt. The largest error in reproducing the experimental $\ln C_{sat}$ is 0.17.

For Rhy2 (with 3.6 wt% H_2O and $M = 1.44$) at 0.5 GPa, the three data points on zircon solubility can be fit as:

$$\ln C_{sat} = (10.517\pm0.282) - (16580\pm411)/T, \quad r^2 = 0.9988 \qquad (6d)$$

The standard state reaction enthalpy is 138±3 kJ/mol, similar to that in Rhy1 (0.12 wt% H_2O) and Rhy5 (5.5 wt% H_2O). The largest error in reproducing the experimental $\ln C_{sat}$ is 0.05.

All the above data in this work show a relatively high and constant standard state reaction enthalpy for zircon dissolution, 138-148 kJ/mol at 0.5 to 1.5 GPa, significantly higher than 84.0±0.3 kJ/mol by Boehnke et al. (2013). This will be discussed further.

For Rhy3 (with 1 wt% H_2O and M = 1.41), there are only two points. A linear fit is nonetheless carried out:

$$\ln C_{sat} = 11.105 - 17997/T. \quad (6e)$$

The error on the fitting parameters cannot be constrained because the straight line is drawn through only two points.

DISCUSSION

Zr diffusion in silicate melts

Comparison of Zr diffusivity with Eyring diffusivity. As a high-valence cation, Zr^{4+} diffusivity is often thought to be not too different from the Eyring diffusivity (Eyring, 1936; Dingwell, 1990; Mungall and Dingwell, 1997; Zhang et al., 2010), which is expressed as:

$$D_{Eyring} = k_B T/(\eta l), \quad (7)$$

where k_B is Boltzmann constant, η is viscosity, and l is the jumping distance of the diffusing species, taking to be 0.3 nm for Zr. To estimate the Eyring diffusivity, viscosity is calculated from the model of Hui and Zhang (2007), which has been shown by Wang et al. (2009) to work well for silicic melts (see figure 9 in Wang et al., 2009).

Fig. 6a shows calculated Eyring diffusivities for Rhy1 (0.12 wt% H_2O) and Rhy5 (5.5 wt% H_2O) as dashed lines. Fig. 8a compares our 0.5-GPa Zr diffusion data with Eyring diffusivity, showing that Zr diffusivity is not too different from Eyring diffusivity. In Fig. 8b,

literature Zr diffusion data in rhyolitic melts are also included in the comparison: the general trends are in agreement but scatter is significant (orders of magnitude).

Dependence of D_{Zr} on temperature and melt composition (including H_2O content) in our experiments. In modeling diffusion data, the temperature effect for a given melt is relatively easy (Arrhenius relation). The pressure effect is handled by using a P/T in the expression of ln$D$ for a single melt (e.g., Zhang, 2008, p. 63-64). The H_2O content has the largest effect among the components, about one lnD_{Zr} unit per wt% H_2O as shown earlier. After some trials, we found that using Si+Al on wet basis (Yu et al., 2015), meaning that H_2O is included in the calculation of cation mole fractions in a similar fashion as Na_2O, roughly accounts for the effect of H_2O as well as the small differences in the anhydrous melt composition in our study. The equation to fit all our D_{Zr} data is:

$$\ln D_{Zr} = \underset{\pm 0.90}{-14.42} - [\underset{\pm 1970}{38784}(\mathrm{Si+Al}) - \underset{\pm 417}{1836}P - \underset{\pm 1478}{3172}]/T, \qquad r^2 = 0.990 \tag{8}$$

where D_{Zr} is in m^2/s. The 1σ errors of the fitting parameters are given at the line below the equation. The maximum error of the above equation in predicting Zr diffusion data in dry and hydrous rhyolitic melts in this study at 1270 to 1885 K and 0.5 to 1.5 GPa is 0.59 ln$D$ units, and the 1σ standard deviation is 0.29 ln$D$ units. That is, the above relatively simple equation works well for all our data in rhyolitic melts (not including data on Rhy4).

The limited success above by using Si+Al cation mole fraction on wet basis to handle the effect of H_2O on Zr diffusivity suggests that Zr diffusivity in a dry basaltic melt is similar to that in a wet high-silica rhyolitic melt containing about 7 wt% H_2O at the same temperature. This relation also roughly holds for melt viscosity: the viscosity of a dry basaltic melt is similar to that of a wet high-silica rhyolitic melt containing about 7 wt% H_2O at the same temperature.

Comparison and combination with literature Zr diffusion data. There is a large data set on Zr diffusion in various silicate melts in the literature (Zhang et al., 2010). Harrison and Watson (1983) studied Zr diffusion during zircon dissolution in LCO rhyolitic melt (Table 1) at 0.8 GPa and up to 6.3 wt% H_2O. Baker and Watson (1988) reported Zr diffusivities in diffusion couple experiments of rhyolites containing F and Cl. Mungall et al. (1999) investigated Zr tracer diffusivity using diffusion couple experiments in a haplogranitic melt HPG8 (Table 1) at 1 bar for dry melt and 1 GPa for HPG8 containing 3.6 wt% H_2O. Baker et al. (2002) determined Zr diffusivities during zircon dissolution in LCO melt and other melts with or without F and Cl.

Zr diffusion in other melts has also been investigated. LaTourrette et al. (1996) investigated Zr diffusion in a haplobasaltic melt. Nakamura and Kushiro (1998) examined Zr diffusion in jadeite melt. Koepke and Behrens (2001) studied Zr diffusion in dry and wet andesitic melt. Lundstrom (2003) reported a single Zr diffusivity in a basaltic melt. Behrens and Hahn (2009) determined Zr diffusivity in potassium-rich trachytic and phonolitic melts. Together with our data, there are 117 Zr diffusivity values in melts from rhyolitic to basaltic and from dry to wet melts.

Although eq. (8) reproduces our own experimental data well, using it to predict Zr diffusion data in silicic melts in other studies would leads to large errors, with maximum error of 1.2 ln$D$ units for Zr diffusion data in halogen-free melts by Baker et al. (2002), 1.5 ln$D$ units for Zr diffusion data in HPG8 and HPG8+3.6wt% H_2O by Mungall et al. (1999), 1.7 ln$D$ units for Zr diffusion data in halogen-bearing melts by Baker et al. (2002), 2.4 ln$D$ units for Zr diffusion data in dry and wet LCO by Harrison and Watson (1999), and 3.0 ln$D$ units for Zr diffusion data in halogen-bearing rhyolitic melts by Baker and Watson (1988). The large errors in using eq. (8) to

predict Zr diffusivity in the other studies mean that there are unaccounted factors in the dependence of Zr diffusivity by eq. (8), including more compositional parameters, larger uncertainties in H_2O contents in early studies, and possible inter-laboratory differences.

When exploring whether other compositional parameters are needed, it is better to use data spanning a large melt composition range. Hence, we made much effort to try to model the whole dataset (including rhyolite, basalt, andesite, jadeite, phonolite, and trachyte melts). In such modeling, the Holy Grail is to determine the compositional effect including the effect of H_2O, which is notoriously difficult to quantify even with many data (e.g., Zhang, 2010; Zhang and Ni, 2010; Zhang et al., 2010). First, we recognize the pressure effect depends on the melt composition: for highly polymerized melt (high Si+Al), viscosity decreases (Kushiro, 1980) and Zr diffusivity increases with pressure (this work); for depolymerized melt (low Si+Al), viscosity increases (Kushiro, 1980) and Zr diffusivity should decrease with pressure. We hence use a term P(Si+Al-a)/T to express lnD_{Zr}, where P is pressure, T is temperature, and a is a constant to be determined by fitting. For additional compositional effects, the effect of Si+Al is easy to determine, but the effect of other components are subtle and more difficult to identify. We also tried to separate the Si and Al effect, but the coefficients for Si term and Al term are identical within error. After numerous trials and after excluding 5 outlier points (two from Harrison and Watson, 1983; one from Baker, 1988; one from Baker et al., 2002; and one from Behrens and Hahn 2009), the following expression is obtained:

$$\ln D_{Zr} = \underset{\pm 0.73}{-13.95} + \underset{\pm 0.84}{5.15}(H+4.1Ca-Mg) - [\underset{\pm 1414}{36457}(Si+Al-1.8Fe) - \underset{\pm 2195}{11008}P(Si+Al-2/3)]/T, \quad (9)$$

where Si, Al, Fe, Mg, Ca and H are cation mole fractions on wet basis (treating H_2O the same as Na_2O), D_{Zr} is in m^2/s, and $r^2 = 0.958$. In calculating the cation mole fractions, Mn, P and the halogens are not counted because their concentrations are low and sometimes these

concentrations are not reported. The 1σ standard deviation of the above equation in predicting 112 data points is 0.71 lnD_{Zr} units (or 0.31 logD_{Zr} units), and the maximum deviation is 1.49 ln$D$ units (or 0.65 log$D$ units). The uncertainty is still relatively large, partially due to the need to better quantify the compositional effect, and partially due to experimental uncertainties and possible inter-laboratory inconsistencies. The five excluded points are off from the above equation by up to 2.1 ln$D$ units. Because the standard deviation of the general equation (9) is more than two times that for specific melts, it is advised that if equations for specific melts are available, it is better to use the specific equations. The general equation may be used to roughly estimate Zr diffusivity in rhyolitic to basaltic melts for which Zr diffusivity has not been determined.

Zircon solubility in silicate melts

Our study also provides data on zircon solubility. There is a large literature on zircon solubility and major efforts were made before to produce models to predict zircon solubility as a function of temperature and melt composition (e.g., Watson, 1979; Dickinson and Hess, 1982; Harrison and Watson, 1983; Watson and Harrison, 1983; Ellison and Hess, 1986; Keppler, 1993; Baker et al., 2002; Rubatto et al., 2007; Boehnke et al., 2013). Importantly, Boehnke et al. (2013) recently reanalyzed the experimental charges and also updated the zircon saturation model by Watson and Harrison (1983). They evaluated the effects of anhydrous melt composition, H_2O content, and pressure, and found that the pressure and H_2O content do not affect zircon solubility significantly, and the parameter M (cation mole fraction ratio of (Na+K+2Ca)/(Al·Si)), which Watson and Harrison (1983) conjured, provides the best

parameterization of the compositional effect. The model by Boehnke et al. (2013) for zircon solubility cast in terms of the partition coefficient of Zr between zircon and silicate melts is:

$$\ln K_d = (10108\pm32)/T - (1.16\pm0.15)(M-1) - (1.48\pm0.09), \quad (10)$$

where $K_d = C_{Zr}^{zircon} / C_{Zr}^{melt}$ and is Zr partition coefficient between zircon and melt, T is temperature in K and M is the cation mole fraction ratio of (Na+K+2Ca)/(Al·Si). If the equation of Boehnke et al. (2013) is used to predict Zr partition coefficient of the ZrO_2 concentration at zircon saturation, the maximum error is 0.82 $\ln C_{sat}$ units. That is, the prediction is not bad even though in detail, the slope (standard state reaction enthalpy) based on Boehnke et al. (2013) is smaller compared to our data (Fig. 7), and our data show noticeable effect of pressure and H_2O content.

To examine possible dependence of K_d on pressure and H_2O content, we define a new parameter Z such that

$$Z = \ln K_d + (1.16\pm0.15)(M-1). \quad (11)$$

If eq. (10) works well, Z should be a function of temperature only and independent of pressure, H_2O content, and M (or other compositional parameters). We examine zircon solubility data from this study, Boehnke et al. (2013), Rubatto and Hermann (2007), Baker et al. (2002), Keppler (1993), Ellison and Hess (1986), Harrison and Watson (1983), and Dickinson and Hess (1982) by plotting Z vs. $1000/T$ (Fig. 9). The data in Watson and Harrison (1983) are not used because Boehnke et al. (2013) reanalyzed most of these samples and updated the data.

In Fig. 9a, data from this study are shown. The details of pressure and H_2O content are not shown in this figure. Overall, the data can be fit by a straight line (solid red line) although there is some scatter. The slope of the straight line is 14.535, larger than 10.108 given by Boehnke et al. (2013). Fig. 9b adds data from Ellison and Hess (1986) and Keppler (1993),

which are consistent with the line in Fig. 9a. The data by Baker et al. (2002) are examined in Fig. 9c and those from Harrison and Watson (1983) are shown in Fig. 9d. All of these data seem to be fairly consistent with the solid red line obtained by fitting data from this work. The data from Boehnke et al. (2013) are included in Fig. 9e, and these data clearly show a smaller slope in Z vs. $1/T$. Fig. 9f adds data from Rubatto and Hermann (2007) and Dickinson and Hess (1982), which display more scatter to the trend of Z vs. $1/T$. When all data are fit by a linear equation, the fit (black solid line) is similar to that defined by eq. (10) (cyan dashed line). Therefore, it seems that if we use M to characterize the compositional dependence and don't consider the effect of pressure and H_2O, the equation by Boehnke et al. (2013) is close to the best approximation, and our new data do not change their equation significantly. When using the equation of Boehnke et al. (2013) to predict $\ln K_d$, our data can be reproduced to within 0.82 $\ln K_d$ units. The largest errors occur for a lunar basaltic melt (Dickinson and Hess, 1982), up to 3 $\ln K_d$ units, which is not surprising because of the compositional difference between lunar basalts and terrestrial melts (such as high FeO and TiO_2 and low Al_2O_3, SiO_2, and alkalis).

Even though the new equation by Boehnke et al. (2013) roughly describes the general trend, using it to predict temperatures in our experiments still has large errors. For example, if eq. (10) is used to predict temperature in our experiments, the largest error is 286 K for ZirDis1 and the second largest error is 232 K for ZirDis7 in our experiments. There is hence a need to incorporate the small effects of H_2O and pressure as well as other compositional parameters on Zr partition coefficient between zircon and silicate melts. Examining Figs. 9e and 9f, it is clear that the data by Boehnke et al. (2013) lead to a smaller slope (temperature dependence) on Z vs. $1/T$ plot compared to data from this study. The experiments in Boehnke et al. (2013) are mostly at lower temperatures and higher H_2O (3-12 wt% H_2O based on either H_2O solubility, or the

amount of H_2O sealed in the capsule, or the difference-from-100% method). One may argue that the slope (or the standard state reaction enthalpy) depends on H_2O content or temperature. However, the datum by Keppler (1993) is also at low temperatures and high H_2O (about 6.1 wt% for H_2O saturation at 0.2 GPa) but it is consistent with the higher slope based on our data. The solubility data in this study at 5.5 wt% H_2O also has a high slope (eq. 6c). Hence, it is not clear why there is a large difference in the slope.

We explored various other approaches to improve the zircon saturation model. The *M* parameter could potentially run into difficulties because the product of Al and Si is in the denominator. For example, Zr concentration at zircon saturation in a synthetic Al-free silicate melt is finite but the *M* parameter would be infinity. Hence, we explored approaches without using the *M* parameter.

Thermodynamically, the equilibrium constant of reaction (5) can be written as:

$$K = a_{ZrO_2}^{melt} a_{SiO_2}^{melt} = X_{ZrO_2}^{melt} X_{SiO_2}^{melt} \gamma_{ZrO_2}^{melt} \gamma_{SiO_2}^{melt}, \quad (12)$$

where a, X, and γ stand for activity, mole fraction and activity coefficient. Hence, theoretically it might be thought that a_{SiO_2} (based on rhyolite-MELTS, Gualda et al., 2012) should play a major role in controlling ZrO_2 concentration at zircon saturation, but experimental data do not show a strong correlation between K_d and a_{SiO_2}.

Another approach is to use a regular solution mixing model for multi-component silicate melts, in which the expression for $\ln \gamma_{ZrO_2}^{melt}$ would contain terms such as X_iX_j where X_i and X_j are mole fractions of component *i* and *j*. We hence explored forms such as:

$$\ln(X_{ZrO_2}^{melt} X_{SiO_2}^{melt}) = A + B/T, \quad (13)$$

where A and B are functions of X_iX_j. Even with many terms, these expressions still have large errors in reproducing the experimental data (e.g., more than 1 $\ln C_{sat}$ units) and the improvement compared to the model of Boehnke et al. (2013) is deemed too small for presentation.

We also considered models treating Zr in melts to be present in various Zr complexes, such as $ZrSiO_4$(melt), $ZrTiO_4$(melt), and $CaZrO_3$(melt) (note that the mineral lakargiite has the composition of $CaZrO_3$), but the results are not satisfying either.

In summary, our extensive search to improve the zircon saturation model was not successful. It is possible that the data from different laboratories have large inconsistencies, or the compositional effects are highly nonlinear in $\ln C_{sat}$ vs composition. If a simple and approximate model is needed, the Boehnke et al. (2013) model is still the best choice so far although the model does have large uncertainties. If data are available for specific melts, it is better to use expressions for specific melts.

Zircon dissolution or growth rates in magma

In a rhyolitic melt, zircon may either dissolve or grow depending on whether Zr concentration in the melt is lower or higher than the saturation concentration, with the latter depending on temperature. The dissolution or growth rate is partially controlled by mass transfer, which may be diffusive or convective for a freely falling zircon crystal (Zhang et al., 1989; Kerr, 1995; Zhang and Xu, 2003). Because zircon crystal is typically small, and rhyolitic melt viscosity is high, one might guess that the settling of zircon in rhyolitic melt is negligibly slow and Zr mass transfer may be treated as diffusive. To quantify, we evaluate the compositional Peclet number defined as:

$$\text{Pe} = (\text{convective mass transfer rate})/(\text{diffusive mass transfer rate}) = 2au/D, \quad (14)$$

where a is the radius of zircon, u is the settling velocity of zircon in the melt, and D is the diffusivity of Zr in the melt. When Pe >> 1, mass transfer is convective. When Pe << 1, mass transfer is diffusive. To estimate Pe, it is necessary to estimate the settling velocity u. When the Reynolds number $\mathrm{Re} = 2au\rho_m/\eta < 1$, u of zircon can be calculated from the Stokes' law:

$$u = 2ga^2\Delta\rho/(9\eta). \quad (15)$$

where g is acceleration due to Earth's gravity (≈ 9.8 m/s^2), $\Delta\rho$ is the density difference between zircon and rhyolitic melt (≈ 2400 kg/m^3), and η is the viscosity of the melt. Hence,

$$\mathrm{Pe} = 4ga^3\Delta\rho/(9\eta D). \quad (16)$$

Because ηD appears together in the denominator and because estimating η and D in a given melt is not trivial, we simplify eq. (16) by using the very rough Eyring relation so that $\eta D = k_B T/l$. Using this very rough approximation, Pe = 1 when $a \approx 17$ μm at 1123 K. That is, zircon dissolution or growth rate in a melt needs to be treated as convective (Kerr, 1995) when zircon radius is of the order 10 μm or more. The convective growth or dissolution rate of a sinking zircon crystal can be calculated as (Kerr, 1995; eq. 4-125 in Zhang, 2008):

$$|\mathrm{d}a/\mathrm{d}t| = \beta D_{Zr}/\delta, \quad (17)$$

where $\beta = (\rho_{melt}/\rho_{zircon})(C_{saturation}-C_{initial})/(C_{Zr\ in\ zircon}-C_{saturation})$ with ρ being density and C being Zr concentration (e.g., in ppm), and δ is the compositional boundary layer thickness on a sinking zircon crystal and can be estimated as

$$\delta = 2a/[1+(1+\mathrm{Pe})^{1/3}], \quad (18)$$

when $\mathrm{Re} \leq 1$ and when steady state is reached for diffusive and convective dissolution or growth of a sinking zircon crystal (Kerr, 1995). The accuracy of the calculated growth or dissolution rate using the above approach has been verified experimentally in various studies (e.g., Kerr, 1995; Zhang and Xu, 2003; Zhang, 2005; Zhang and Xu, 2008; also see review by Zhang, 2013)

to be about 15% relative. If zircon growth is diffusion controlled, using eq. (17) would mostly overestimate zircon growth rate.

One specific example for the calculation of zircon dissolution or growth rate is given below. For better accuracy, diffusivity and solubility equations for specific melt are used. Consider a zircon crystal with a radius of 30 μm in a Rhy5 melt containing 5.5 wt% H_2O and 130 ppm Zr at 1173 K and 0.5 GPa (130 ppm Zr is the concentration in this hydrous natural obsidian). Zr concentration at zircon saturation can be estimated using eq. (6c) to be 193 ppm. Hence, zircon is undersaturated and would dissolve in the melt, and the dissolution rate can be calculated using eq. (17). The viscosity in the melt can be roughly estimated from Hui et al. (2007) to be $\eta = 7000$ Pa·s. The falling velocity (Stokes' velocity) $u = 6.7\times10^{-10}$ m/s = 0.021 m/yr. The Reynolds number $\mathrm{Re} = 2au\rho_m/\eta = 1.3\times10^{-14} \ll 1$, meaning that Stokes' law applies. Zr diffusivity can be estimated from eq. (4c) to be 7.4×10^{-15} m^2/s. Hence, the Peclet number $\mathrm{Pe} = 2au/D = 5.4$. Thus, the boundary layer thickness is about 21 μm. Therefore, the dissolution rate can be calculated using eq. (17) to be 2.2×10^{-14} m/s, or 0.68 μm/yr. The zircon crystal would survive in the melt at 1173 K for no more than 50 years. The survival time would increase if the melt contains less H_2O (leading to smaller Zr diffusivity) or if the initial Zr concentration is closer to the saturation concentration. The three most critical factors for zircon survival in a magma are temperature, H_2O concentration in the melt, and Zr concentration in the melt. As temperature decreases, the diffusivity decreases, slowing the kinetics. As H_2O concentration in the melt increases, Zr diffusivity increases, enhancing the kinetics. More importantly, Zr concentration at zircon saturation decreases as temperature decreases so that zircon may not dissolve at all, and may grow. For example, if we repeat the same calculation for a zircon crystal of 30 μm radius in Rhy5 melt with 5.5 wt% H_2O and 130 ppm Zr at 0.5 GPa but

at 1123 K, Zr concentration at zircon saturation would be 102 ppm, and zircon would grow at a rate of ~0.12 μm/yr.

Figure 10 shows calculated zircon dissolution/growth rate as a function of temperature and Zr concentration in Rhy5 with 5.5 wt% H_2O. It can be seen that zircon dissolution rate can be high when the temperature is high, but zircon growth rate is typically low: In Rhy5 with 5.5 wt% H_2O, the maximum growth rate changes from 0.086 μm/yr for 100 ppm Zr in the melt to 0.46 μm/yr for 200 ppm Zr in the melt. Zircon growth rate decreases by orders of magnitude in dry rhyolitic melts: In Rhy1 with 0.12 wt% H_2O, the maximum growth rate changes from 7.1×10^{-5} μm/yr for 100 ppm Zr in the melt to 0.00054 μm/yr for 200 ppm Zr in the melt. That is, typical zircon growth rate in wet rhyolitic melts is ≤1 μm/yr, and much slower in dry rhyolitic melts.

For a given Zr concentration in a specific melt, there is a maximum zircon growth rate (Fig. 10). The maximum zircon growth rate depends on Zr concentration in a given melt, and our calculations show that it is a power function of Zr concentration (Fig. 11). For example, for Rhy5 with 5.5 wt% H_2O, the maximum zircon growth rate can be roughly estimated as $1.30C_\infty^{2.406}$ μm/Myr where C_∞ is Zr concentration in ppm in the initial (or far-field) melt. For Rhy1 with 0.12 wt% H_2O, the maximum zircon growth rate can be roughly expressed as $0.00010C_\infty^{2.926}$ μm/Myr (Fig. 11). At the same Zr concentration, the maximum zircon growth rate in the hydrous melt Rhy5 is about 3 orders of magnitude higher than that in the dry melt Rhy1. To have similar maximum growth rate, a dry melt such as Rhy1 with 0.12 wt% H_2O must have a Zr concentration that is 14 times that in a wet melt Rhy5 with 5.5 wt% H_2O.

Zircon crystal size as a geospeedometer

The quantification of zircon growth rate as a function of temperature may be inversed to provide a rough estimate of the upper limit of cooling rate of a magma based on the size of zircon crystals in a rock. Still using Rhy5 containing 5.5 wt% H_2O as an example. Assume that zircon grows as it sinks in an infinite melt volume without other crystals present, meaning that the growth rate is the upper limit because the presence of other crystals especially other zircon crystals limits the growth rate. Therefore, the estimated cooling rate using this approach is also an upper limit. Also assume that the melt composition and H_2O concentration do not change during zircon growth (this is clearly a simplification). It is necessary to know the saturation temperature of zircon based on Zr concentration evolution in the melt. Suppose zircon saturation temperature is 1123 K in a differentiated melt whose composition is the same as Rhy5. That is, at 1123 K the differentiated melt contains 102 ppm Zr. Using the method for convective crystal growth during cooling (as described in detail in Zhang, 2015), if the cooling time scale τ (T decreases with t as $T_0 e^{-t/\tau}$, the initial cooling rate is T_0/τ; see Zhang, 1994) is 1000 yrs, the final zircon radius would be 19.5 μm. If the cooling time scale is 3000 yrs, the final zircon radius would be 37.5 μm. If the cooling time scale is 10000 yrs, the final zircon radius would be 86.3 μm. Hence, knowing Zr saturation temperature and final zircon radius, the lower limit of the cooling time scale or the upper limit of the cooling rate can be roughly estimated.

The above calculation is for a wet rhyolitic melt Rhy5. Because zircon growth rate in dry rhyolitic melt is slower by 3 orders of magnitude than in Rhy5 (Fig. 11), large zircon crystals require special conditions to form, including high Zr concentration (e.g., > 200 ppm Zr) in the melt, and very long lifetime of the magma chamber.

Zircon geospeedometer applied to Bishop Tuff

The geospeedometer outlined above is now applied to Bishop Tuff in which zircon is one of the early formed minerals (Hildreth, 1979). Bishop Tuff pumice composition is similar to Rhy5, with similar H_2O content (Hildreth, 1979; Skirius et al., 1990; Lu et al., 1992; Wallace et al., 2003). Because the early Bishop Tuff is crystal-poor abut the late Bishop Ruff is crystal-rich (Hildreth and Wilson, 2007), the simple model of convective zircon growth in an infinite melt is better applied to the early Bishop Tuff than the late Bishop Tuff. Because crystallinity is low and crystallization occurs near granite minimum composition with multi-phase saturation, melt composition change with crystallization may be ignored. Zr concentration in early Bishop Tuff melt inclusions hosted by quartz is about 90 ppm (Lu et al., 1992). Using Rhy5 to approximate Bishop Tuff melt, zircon crystallization begins at 1114 K (840°C). Zircon crystal diameter in early Bishop Tuff can be as large as 200 μm (Bindeman, 2003). Assume these to be indigenous crystals. Using the convective crystal growth model outlined above to estimate zircon growth during magma cooling (Zhang, 2015), the cooling time scale must be ~17 kyr to grow a zircon crystal of 200 μm diameter (100 μm radius). Note that this is a lower limit of the cooling time scale. Also note that the cooling time scale of the magma chamber is different from the time needed to grow a large zircon crystal (the residence time of a large zircon crystal in the magma) because eruption occurred before cooling down. Adopting an eruption temperature of 1000 K (Hildreth, 1979), a magma chamber cooling time scale of 20 kyr is estimated to grow 200-μm zircon crystals at the time and temperature of eruption, and the growth time (or residence time) of zircon is 2.2 kyr (i.e., it took 2.2 kyr for the magma chamber to cool from 1114 K to 1000 K).

A minimum zircon residence time can be estimated using the maximum zircon growth rate for the given Zr concentration in the initial melt. The maximum zircon growth rate during cooling is 0.071 μm/yr for a Zr concentration of 90 ppm in Rhy5. Even if the magma chamber is

maintained at the temperature of maximum growth rate, a zircon crystal of 100 μm radius would still require 1.4 kyr to grow. Hence, within the context of our zircon geospeedometer, zircon residence time in the Bishop Tuff magma chamber is 1.4 to 2.2 kyr. The use of our zircon geospeedometer adds new constraints to the debate on the residence time of zircon crystals in Bishop Tuff magma chamber (e.g., Reid and Coath, 2000; Crowley et al., 2007).

CONCLUSIONS

We conducted zircon dissolution experiments in several rhyolitic melts to investigate zircon saturation condition and zircon dissolution kinetics. Both Zr diffusivity and zircon solubility depends strongly on temperature and weakly on pressure and anhydrous melt composition. Zr diffusivity also increases strongly with H_2O concentration in the melt, about 1 ln$D$ unit per wt% H_2O. On the other hand, the effect of H_2O on zircon solubility is small, about 0.05 lnC_{sat} units per wt% H_2O. For individual rhyolitic melts, Zr diffusivity can be predicted fairly well, typically within 0.4 lnD_{Zr} units; and zircon solubility can be predicted within 0.17 lnC_{sat} units. A general Zr diffusivity model for basaltic to rhyolitic melts is constructed, but the error in reproducing the experimental data is relatively large. For zircon solubility, even though effort was made, we were not able to significantly improve the recent model of Boehnke et al. (2013). Our data show that zircon solubility increases as pressure decreases, leading to decompressional zircon dissolution in melt. Zircon dissolution and growth rate in specific rhyolitic melts can be estimated, and zircon dissolution and growth rate depends largely on (i) the temperature, which determines Zr diffusivity and zircon solubility, (ii) H_2O content in the melt, which has a large effect on Zr diffusivity, and (iii) Zr concentration in the melt. Zircon

growth rate in rhyolitic melts is typically slow, ≤ 1 μm/yr. The ability to estimate zircon growth rate also offers a tool to estimate the upper limit of the cooling rate of a magma. The presence of large indigenous zircon crystals in Bishop Tuff indicates that the cooling time scale for the Bishop Tuff magma chamber is ≥ 17 kyr and zircon growth time of 1.4 to 2.2 kyr.

ACKNOWLEDGEMENTS

We thank James Mungall and an anonymous reviewer for insightful and constructive comments. This work was supported by US NSF grant EAR-0838127, EAR-1019440, and EAR-1524473. The electron microprobe at the University of Michigan was purchased with NSF grant EAR-9911352.

REFERENCES CITED

Baker, D.R., Conte, A.M., Freda, C., and Ottolini, L. (2002) The effect of halogens on Zr diffusion and zircon dissolution in hydrous metaluminous granitic melts. Contributions to Mineralogy and Petrology, 142, 666-678.

Baker, D.R., and Watson, E.B. (1988) Diffusion of major and trace elements in compositionally complex Cl- and F-bearing silicate melts. Journal of Non-Crystalline Solids, 102, 62-70.

Behrens, H., and Hahn, M. (2009) Trace element diffusion and viscous flow in potassium-rich trachytic and phonolitic melts. Chemical Geology, 259, 63-77.

Bindeman, I.N. (2003) Crystal sizes in evolving silicic magma chambers. Geology, 31, 367-370.

Boehnke, P., Watson, E.B., Trail, D., Harrison, T.M., and Schmitt, A.K. (2013) Zircon saturation re-visited. Chemical Geology, 351, 324-334.

Chen, Y., and Zhang, Y. (2008) Olivine dissolution in basaltic melt. Geochimica et Cosmochimica Acta, 72, 4756-4777.

Chen, Y., and Zhang, Y. (2009) Clinopyroxene dissolution in basaltic melt. Geochimica et Cosmochimica Acta, 73, 5730-5747.

Crowley, J.L., Schoene, B., and Bowring, S.A. (2007) U-Pb dating of zircon in the Bishop Tuff at the millennial scale. Geology, 35, 1123-1126.

Dickinson, J.E., and Hess, P.C. (1982) Zircon saturation in lunar basalts and granites. Earth and Planetary Science Letters, 57, 336-344.

Dingwell, D.B. (1990) Effects of structural relaxation on cationic tracer diffusion in silicate melts. Chemical Geology, 82, 209-216.

Ellison, A.J., and Hess, P.C. (1986) Solution behavior of +4 cations in high silica melts: petrologic and geochemical implications. Contributions to Mineralogy and Petrology, 94, 343-351.

Eyring, H. (1936) Viscosity, plasticity, and diffusion as examples of absolute reaction rates. Journal of Chemical Physics, 4, 283-291.

Ganguly, J., Bhattacharya, R.N., and Chakraborty, S. (1988) Convolution effect in the determination of

compositional profiles and diffusion coefficients by microprobe step scans. American Mineralogist, 73, 901-909.
Gualda, G.A.R., Ghiorso, M.S., Lemons, R.V., and Carley, T.L. (2012) Rhyolite-MELTS: a modified calibration of MEOLS optimized for silica-rich, fluid-bearing magmatic systems. Journal of Petrology, 53, 875-890.
Hanchar, J.M., and Hoskin, P.W.O. (2013) Zircon. Reviews in Mineralogy and Geochemistry, 53, 1-500.
Hanchar, J.M., and Watson, E.B. (2003) Zircon saturation thermometry. Reviews in Mineralogy and Geochemistry, 53, 89-112.
Harrison, T.M., and Watson, E.B. (1983) Kinetics of zircon dissolution and zirconium diffusion in granitic melts of variable water content. Contributions to Mineralogy and Petrology, 84, 66-72.
Hildreth, W. (1979) The Bishop Tuff: Evidence for the origin of compositional zonation in silicic magma chambers. Geological Society of America Special Paper, 180, 43-73.
Hildreth, W., and Wilson, C.J. (2007) Compositional zoning of the Bishop Tuff. Journal of Petrology, 48, 951-999.
Hui, H., and Zhang, Y. (2007) Toward a general viscosity equation for natural anhydrous and hydrous silicate melts. Geochimica et Cosmochimica Acta, 71, 403-416.
Hui, H., Zhang, Y., Xu, Z., Del Gaudio, P., and Behrens, H. (2009) Pressure dependence of viscosity of rhyolitic melts. Geochimica et Cosmochimica Acta, 73, 3680-3693.
Hui, H., Zhang, Y., Xu, Z., and Behrens, H. (2008) Pressure dependence of the speciation of dissolved water in rhyolitic melts. Geochimica et Cosmochimica Acta, 72, 3229-3240.
Keppler, H. (1993) Influence of fluorine on the enrichment of high field strength trace elements in granitic rocks. Contributions to Mineralogy and Petrology, 114, 479-488.
Kerr, R.C. (1995) Convective crystal dissolution. Contributions to Mineralogy and Petrology, 121, 237-246.
Koepke, J., and Behrens, H. (2001) Trace element diffusion in andesitic melts: an application of synchrontron X-ray fluorescence analysis. Geochimica et Cosmochimica Acta, 65, 1481-1498.
Kushiro, I. (1980) Viscosity, density, and structure of silicate melts at high pressures, and their petrological applications. In Hargraves, Ed. Physics of Magmatic Processes, p. 93-120. Princeton U. Press, Princeton, N.J.
LaTourrette, T., Wasserburg, G.J., and Fahey, A.J. (1996) Self diffusion of Mg, Ca, Ba, Nd, Yb, Ti, Zr, and U in haplobasaltic melt. Geochimica et Cosmochimica Acta, 60, 1329-1340.
Liu, Y., and Zhang, Y. (2000) Bubble growth in rhyolitic melt. Earth and Planetary Science Letters, 181, 251-264.
Liu, Y., Zhang, Y., and Behrens, H. (2005) Solubility of H_2O in rhyolitic melts at low pressures and a new empirical model for mixed H_2O-CO_2 solubility in rhyolitic melts. Journal of Volcanology and Geothermal Research, 143, 219-235.
Lu, F., Anderson, A.T., and Davis, A.M. (1992) Melt inclusions and crystal-liquid separation in rhyolitic magma of the Bishop Tuff. Contributions to Mineralogy and Petrology, 110, 113-120.
Mungall, J.E. (2002) Empirical models relating viscosity and tracer diffusion in magmatic silicate melts. Geochimica et Cosmochimica Acta, 66, 125-143.
Mungall, J.E., and Dingwell, D.B. (1997) Actinide diffusion in a haplogranitic melt: Effects of pressure, water content, and pressure. Geochimica et Cosmochimica Acta, 61, 2237-2246.
Mungall, J.E., Dingwell, D.B., and Chaussidon, M. (1999) Chemical diffusivities of 18 trace elements in granitoid melts. Geochimica et Cosmochimica Acta, 63, 2599-2610.
Newman, S., Epstein, S., and Stolper, E.M. (1988) Water, carbon dioxide, and hydrogen isotopes in glasses from the ca. 1340 A.D. eruption of the Mono Craters, California: Constraints on degassing phenomena and initial volatile content. Journal of Volcanology and Geothermal Research, 35, 75-96.
Newman, S., Stolper, E.M., and Epstein, S. (1986) Measurement of water in rhyolitic glasses: calibration of an infrared spectroscopic technique. American Mineralogist, 71, 1527-1541.
Ni, H., Behrens, H., and Zhang, Y. (2009) Water diffusion in dacitic melt. Geochimica et Cosmochimica Acta, 73, 3642-3655.

Ni, H., and Zhang, Y. (2008) H_2O diffusion models in rhyolitic melt with new high pressure data. Chemical Geology, 250, 68-78.

Reid, M.R., and Coath, C.D. (2000) In situ U-Pb ages of zircons from the Bishop Tuff: no evidence for long crystal residence times. Geology, 28, 443-446.

Rubatto, D., and Hermann, J. (2007) Experimental zircon/melt and zircon/garnet trace element partitioning and implications for the geochronology of crustal rocks. Chemical Geology, 241, 38-61.

Sieh, K., and Bursik, M. (1986) Most recent eruptions of the Mono Craters, eastern central California. Journal of Geophysical Research, 91, 12539-12571.

Simon, J.I., Renne, P.R., and Mundil, R. (2008) Implications of pre-eruptive magmatic histories of zircons for U-Pb geochronology of silicic extrusions. Earth and Planetary Science Letters, 266, 182-194.

Skirius, C.M., Peterson, J.W., and A.T. Anderson, J. (1990) Homogenizing rhyolitic glass inclusions from the Bishop Tuff. American Mineralogist, 75, 1381-1398.

Valley, J.W., Lackey, J.S., Cavosie, A.J., Clechenko, C.C., Spicuzza, M.J., Basei, M.A.S., Bindeman, I.N., Ferreira, V.P., Sial, A.N., King, E.M., Peck, W.H., Sinha, A.K., and Wei, C.S. (2005) 4.4 billion years of crustal maturation: oxygen isotope ratios of magmatic zircon. Contributions to Mineralogy and Petrology, 150, 561-580.

Wallace, P.J., Dufek, J., Anderson, A.T., and Zhang, Y. (2003) Cooling rates of Plinian-fall and pyroclastic-flow deposits in the Bishop Tuff: inferences from water speciation in quartz-hosted glass inclusions. Bulletin of Volcanology, 65, 105-123.

Wang, H., Xu, Z., Behrens, H., and Zhang, Y. (2009) Water diffusion in Mount Changbai peralkaline rhyolitic melt. Contributions to Mineralogy and Petrology, 158, 471-484.

Watson, E.B. (1979) Zircon saturation in felsic liquids: experimental results and applications to trace element geochemistry. Contributions to Mineralogy and Petrology, 70, 407-419.

Watson, E.B., and Harrison, T.M. (1983) Zircon saturation revisited: temperature and composition effects in a variety of crustal magma types. Earth and Planetary Science Letters, 64, 295-304.

Xu, Z., and Zhang, Y. (2002) Quench rates in water, air and liquid nitrogen, and inference of temperature in volcanic eruption columns. Earth and Planetary Science Letters, 200, 315-330.

Yu, Y., Zhang, Y., and Yang, Y. (2015) Diffusion of SiO_2 in rhyolitic melt. AGU Fall Meeting abstract, submitted.

Zhang, Y. (1994) Reaction kinetics, geospeedometry, and relaxation theory. Earth and Planetary Science Letters, 122, 373-391.

Zhang, Y. (1999) H_2O in rhyolitic glasses and melts: measurement, speciation, solubility, and diffusion. Reviews of Geophysics, 37, 493-516.

Zhang, Y. (2005) Fate of rising CO_2 droplets in seawater. Environmental Science and Technology, 39, 7719-7724.

Zhang, Y. (2008) Geochemical Kinetics. 656 p. Princeton University Press, Princeton, NJ.

Zhang, Y. (2010) Diffusion in minerals and melts: theoretical background. Reviews in Mineralogy and Geochemistry, 72, 5-59.

Zhang, Y. (2013) Kinetics and dynamics of mass-transfer-controlled mineral and bubble dissolution or growth: a review. European Journal of Mineralogy, 25, 255-266.

Zhang, Y. (2015) Toward a quantitative model for the formation of gravitational magmatic sulfide deposits. Chemical Geology, 391, 56-73.

Zhang, Y., Belcher, R., Ihinger, P.D., Wang, L., Xu, Z., and Newman, S. (1997) New calibration of infrared measurement of water in rhyolitic glasses. Geochimica et Cosmochimica Acta, 61, 3089-3100.

Zhang, Y., and Ni, H. (2010) Diffusion of H, C, and O components in silicate melts. Reviews in Mineralogy and Geochemistry, 72, 171-225.

Zhang, Y., Ni, H., and Chen, Y. (2010) Diffusion data in silicate melts. Reviews in Mineralogy and Geochemistry, 72, 311-408.

Zhang, Y., Walker, D., and Lesher, C.E. (1989) Diffusive crystal dissolution. Contributions to

Mineralogy and Petrology, 102, 492-513.
Zhang, Y., and Xu, Z. (2003) Kinetics of convective crystal dissolution and melting, with applications to methane hydrate dissolution and dissociation in seawater. Earth and Planetary Science Letters, 213, 133-148.
Zhang, Y., and Xu, Z. (2008) "Fizzics" of bubble growth in beer and champagne. Elements, 4, 47-49.
Zhang, Y., Xu, Z., Zhu, M., and Wang, H. (2007) Silicate melt properties and volcanic eruptions. Reviews of Geophysics, 45, RG4004, doi:10.1029/2006RG000216.

Table 1. Chemical compositions of starting materials (wt% oxide on dry basis)

	Zircon	Rhy1	Rhy2	Rhy3	Rhy4	Rhy5	LCO	HPG8
SiO_2	32.51±0.23	72.80	73.14	75.53	76.48	76.62	76.1	79.64
TiO_2		0.24	0.26	0.09	0.05	0.13	0.1	
Al_2O_3		14.08	14.46	13.12	13.01	13.71	13.0	11.33
FeO(t)		2.16	1.51	1.05	0.91	0.88	0.7	
MgO		0.22	0.31	0.02	0.02	0.11	0.1	
CaO		0.91	1.28	0.55	0.41	0.90	0.5	
Na_2O		5.20	4.20	4.09	4.07	3.64	3.7	4.88
K_2O		4.04	4.58	4.92	5.29	4.54	4.8	4.15
ZrO_2	66.38±0.31	0.0454	0.026	0.013	0.023	0.017		
HfO_2	1.54±0.04							
Dry total	**100.43**	**99.70**	**99.78**	**99.38**	**100.26**	**100.55**	**99.0**	**100.00**
$\log\eta_{dry}$ (Pa·s)		4.72	4.87	5.59	5.70	5.94	5.82	6.25
M		1.54	1.44	1.41	1.43	1.28	1.31	1.44
H_2O		0.12	3.63	1.05	0.24	5.54	~0.1	~0.03

Reported concentrations for zircon are based on 74 analyses of 7 zircon wafers by electron microprobe. Errors are given at 1σ level hereafter. For glasses, the concentrations are based on averages of at least 5 points of electron microprobe analyses except for Rhy1, which is based on ICP-MS analysis. For easy comparison, concentrations are recalculated on dry basis using $C_{dry} = C_{wet}/(1-C_{H2O})$ where C is mass fraction. Concentrations are not normalized to 100%. The last 2 columns list the composition of Lake County obsidian (LCO) used by Harrison and Watson (1983) and Baker et al. (2002) and HPG8 by Mungall et al. (1999) for comparison. η is viscosity for "dry" rhyolitic melt with 0.15 wt% H_2O at 1500K for the purpose of examining the effect of melt composition on Zr diffusivity. M is the cation ratio $M = (Na+K+2Ca)/(Al \cdot Si)$ defined by Watson and Harrison (1983).

Table 2. Experimental conditions and results

Exp#	Melt	T (K)	P (GPa)	Time (s)	H_2O* (wt%)	Capsule	L_c (μm)	C_∞ (wt%)	C_0 (wt%)	D_{Zr} (10^{-14} m^2/s)
ZirDis1	Rhy1	1885	0.47	7325	*0.12*	Graphite	1.94	0.0454	5.17(4)	24.9(5)
ZirDis2	Rhy1	1701	0.47	86363	*0.12*	Graphite	0.73	0.0454	1.55(2)	3.61(9)
ZirDis3	Rhy1	1467	0.5	360126	0.124	Graphite	0.071	0.050	0.374(3)	0.179(6)
ZirDis4	Rhy1	1673	0.5	29024	*0.12*	Graphite	0.40	0.042	1.257(12)	4.86(2)
ZirDis8[#]	Rhy1	1357	0.5	777600	*0.12*	Graphite	0.036	0.058	~0.36	
ZirDis14	Rhy1	1676	1.5	29660	*0.12*	Graphite	0.52	0.050	1.01(5)	13.6(16)
ZirDis15	Rhy1	1890	1.5	7210	*0.12*	Graphite	1.48	0.050	3.28(1)	38.0(3)
ZirDis16	Rhy1	1685	1.5	28900	*0.12*	Graphite	0.50	0.052	1.01(10)	12.4±(1)
ZirDis17[#]	Rhy1	1483	1.5	173002	*0.12*	Graphite	0.079	0.074	~0.32	
ZirDis12	Rhy2	1677	0.5	3630	3.39	Pt	0.82	0.014	1.893(9)	76.0(14)
ZirDis13b	Rhy2	1373	0.5	43048	3.42	Au75Pd25	0.084	0.027	0.209(2)	6.98±(40)
ZirDis18	Rhy2	1468	0.5	21580	*3.63*	Au75Pd25	0.21	0.032	0.431(2)	17.7(4)
ZirDis10	Rhy3	1664	0.5	3041	1.17	Graphite	0.17	0.010	1.319(9)	7.32(14)
ZirDis11	Rhy3	1368	0.5	70693	0.90	Au75Pd25	0.0095	0.016	0.127(4)	0.141(10)
ZirDis9	Rhy4	1569	0.5	172840	*0.24*	Graphite	0.45	0.023	1.318(3)	0.95(1)
ZirDis19[$]	Rhy4	1571	0.5	10832	*0.24*	Graphite	0.029	0.022	~0.743(12)	
ZirDis5	Rhy5	1475	0.5	318	5.50	Au75Pd25	0.040	0.019	0.405(5)	47.8(14)
ZirDis6b	Rhy5	1270	0.5	39569	5.06	Au75Pd25	0.020	0.017	0.083(2)	3.36(36)
ZirDis7	Rhy5	1671	0.5	318	5.76	Pt	0.51	0.017	2.00(1)	290(6)

Compositions of Rhy1, Rhy2, Rhy3, Rhy4 and Rhy5 can be found in Table 1. L_c is zircon dissolution distance based on mass balance. C_∞ is ZrO_2 concentration in the far-field (or initial) melt. C_0 is ZrO_2 concentration in the interface melt. D_{Zr} is Zr diffusivity in the melt. Errors at 1σ level for C_0 and D_{Zr} are given in parentheses on the last digit.

* This is measured total H_2O after experiment except for values in italics, which are those before experiment.

[#] The experimental charge partially crystallized due to low experimental temperature, and the data are not used.

[$] The concentration profile is too short for D_{Zr} to be determined accurately.

This is a preprint, the final version is subject to change, of the American Mineralogist (MSA)
Cite as Authors (Year) Title. American Mineralogist, in press.
(DOI will not work until issue is live.) DOI: http://dx.doi.org/10.2138/am-2016-5462

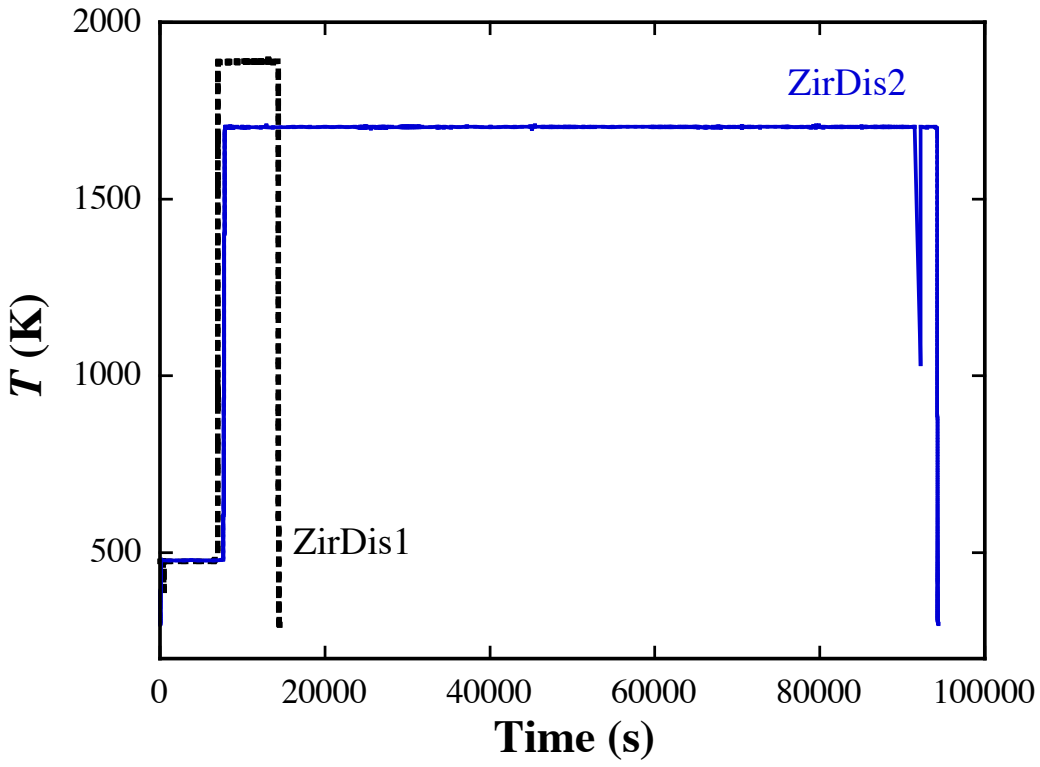

Fig. 1. Temperature history of two experiments. It can be seen that there was a sudden temperature drop by about 670 K for experiment ZirDis2.

This is a preprint, the final version is subject to change, of the American Mineralogist (MSA)
Cite as Authors (Year) Title. American Mineralogist, in press.
(DOI will not work until issue is live.) DOI: http://dx.doi.org/10.2138/am-2016-5462

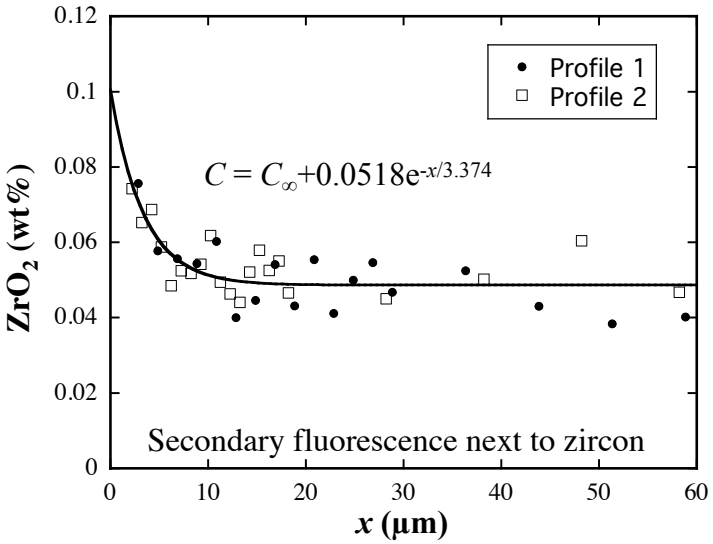

Fig. 2. Secondary fluorescence signal of ZrO_2 in obsidian glass next to zircon. The zircon-glass interface is at $x = 0$. The precision in ZrO_2 analysis is about ±0.01%.

This is a preprint, the final version is subject to change, of the American Mineralogist (MSA)
Cite as Authors (Year) Title. American Mineralogist, in press.
(DOI will not work until issue is live.) DOI: http://dx.doi.org/10.2138/am-2016-5462

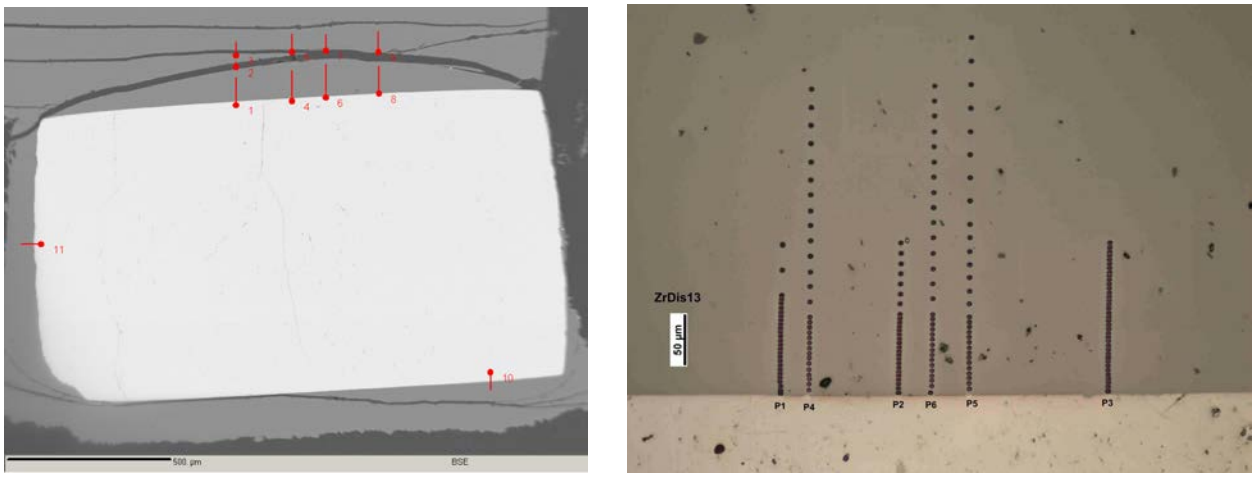

Fig. 3. Left: A BSE image of ZirDis3 (the horizontal scale bar is 500 µm). Zircon is brighter and glass is darker. Four traverses (indicated by red segments) at the upper side of graph are used to extract diffusivity, and the other two short traverses are used to verify ZrO_2 content in the interface melt. The mid-concentration diffusion distance (Zhang, 2008) is 25 µm, and the distance between the interface and the first crack near the center axis is about 100 µm. The interface between zircon and melt (glass) is straight and sharp.

Right: A reflected-light photomicrograph for ZirDis13 (the vertical scale bar is 50 µm). Zircon is brighter and glass is darker. Six traverses with individual microprobe spots can be seen. There are also some pits due to imperfect polishing.

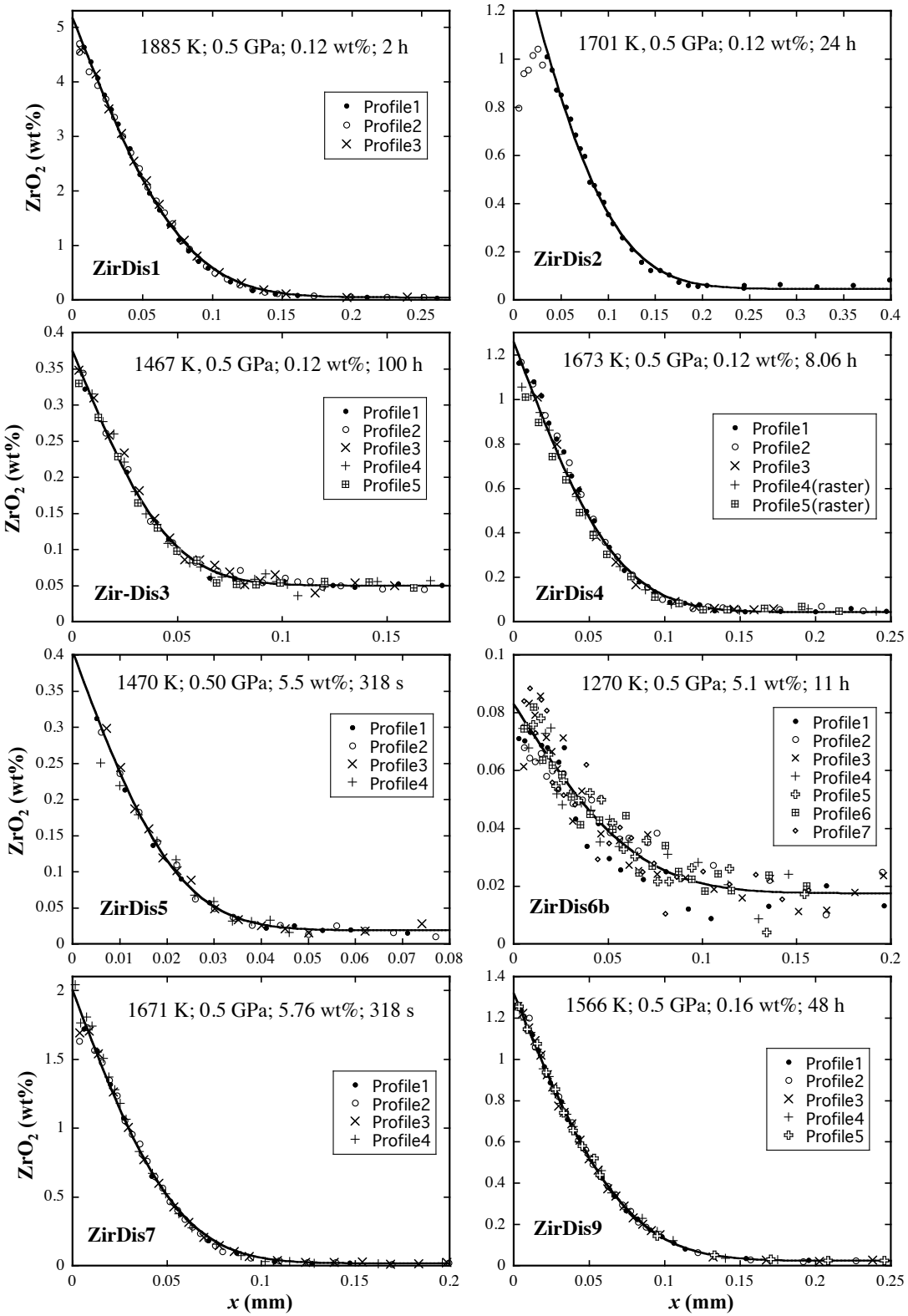

Fig. 4. ZrO_2 concentration profiles for 8 zircon dissolution experiments and fits.

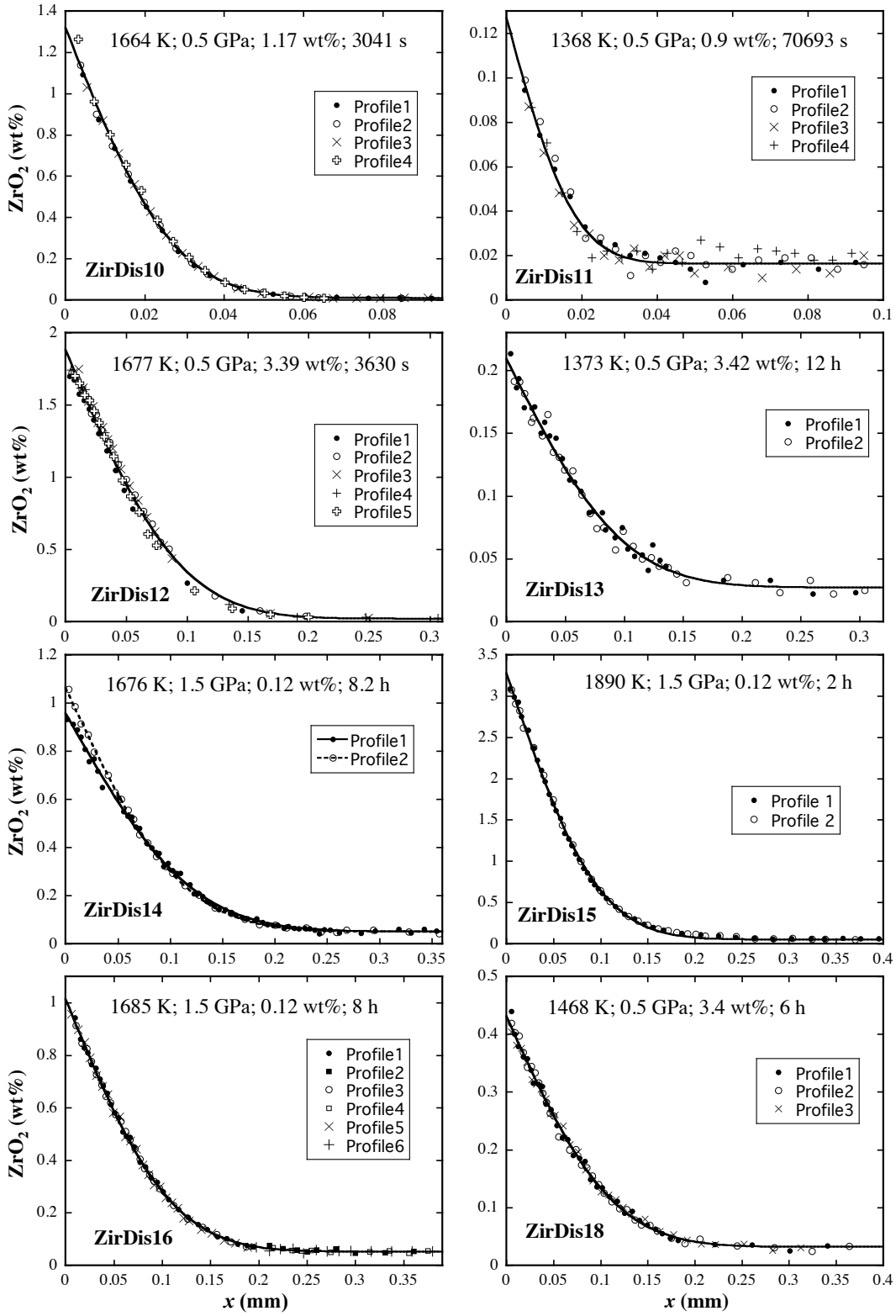

Fig. 5. ZrO_2 concentration profiles for 8 zircon dissolution experiments and fits.

This is a preprint, the final version is subject to change, of the American Mineralogist (MSA)
Cite as Authors (Year) Title. American Mineralogist, in press.
(DOI will not work until issue is live.) DOI: http://dx.doi.org/10.2138/am-2016-5462

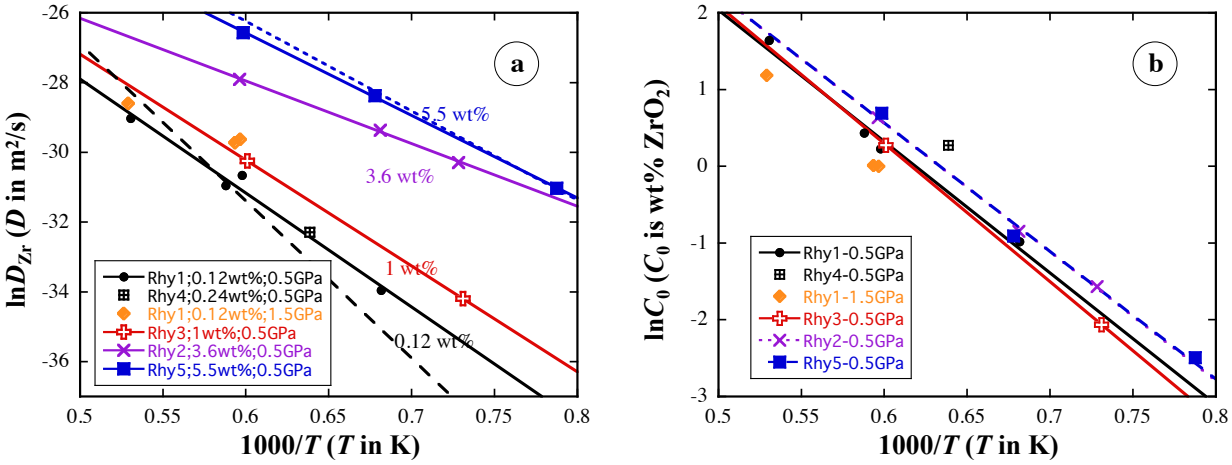

Fig. 6. (a) Experimental data on Zr diffusivity. The solid lines to fit of the respective diffusivity data. The dashed lines of the same color are the Eyring diffusivity (for clarity, only two Eyring diffusivity lines are shown: one for 0.12 wt%, and the other for 5.5 wt% H_2O). (b) Experimental data on interface ZrO_2 concentration (interpreted as zircon solubility). The fit lines (solid or dashed) are the same as the data points.

This is a preprint, the final version is subject to change, of the American Mineralogist (MSA)
Cite as Authors (Year) Title. American Mineralogist, in press.
(DOI will not work until issue is live.) DOI: http://dx.doi.org/10.2138/am-2016-5462

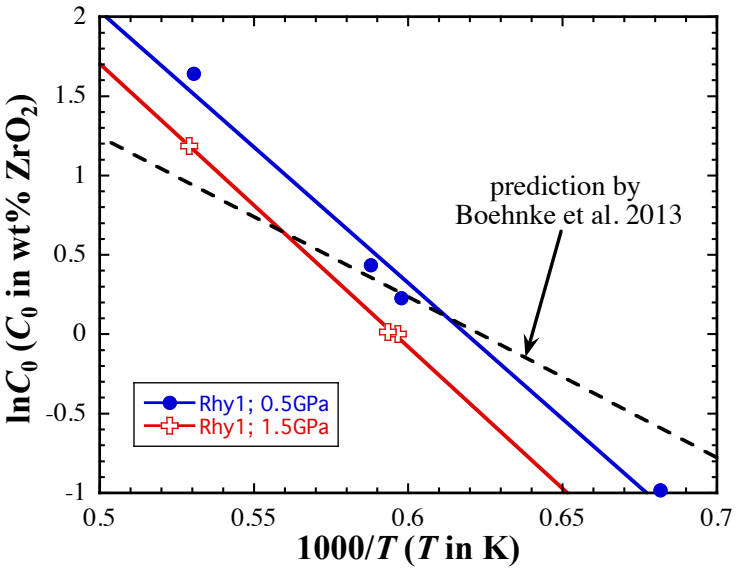

Fig. 7. Zircon solubility in Rhy1 melt at 0.5 GPa and 1.5 GPa. The fit to the 0.5 GPa data are shown as a blue solid line, and the fit to the 1.5 GPa data are shown as a red solid line. The prediction by the model of Boehnke et al. (2013), which is a single line for both 0.5 and 1.5 GPa, is shown as a black dashed line.

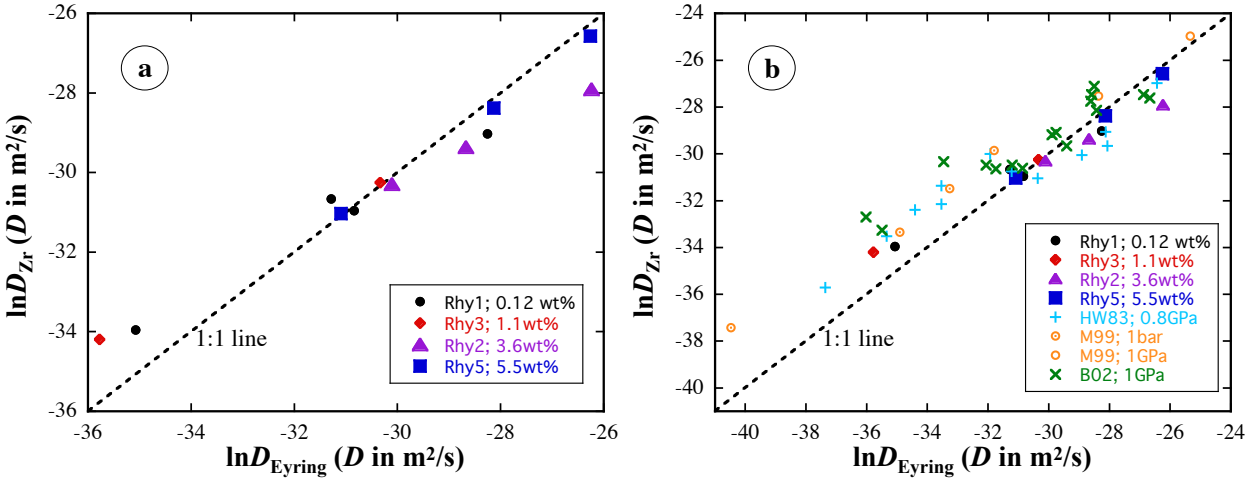

Fig. 8. (a) Our own Zr diffusion data at 0.5 GPa vs. Eyring diffusivity. The 1:1 line is shown as a dashed line. The fit is shown as a solid line. (b) Literature and our Zr diffusion data vs. Eyring diffusivity. HW83: Harrison and Watson (1983); M99: Mungall et al. (1999); B02: Baker et al. (2002). The rest are our data.

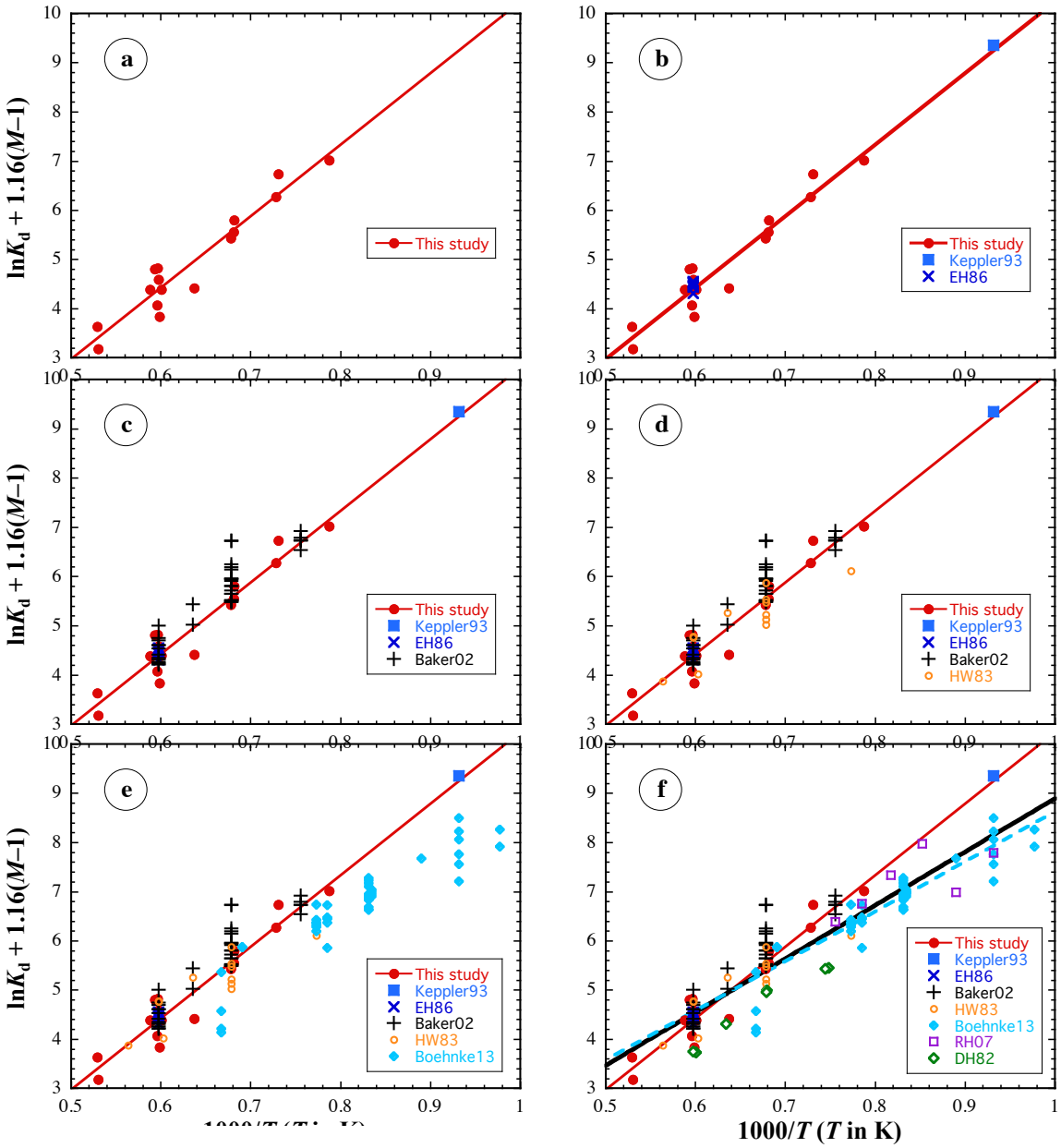

Fig. 9. $Z = \ln K_d + 1.16(M-1)$ vs. $1000/T$ for data in different papers. EH86 = Ellison and Hess (1986). Baker02 = Baker et al. (2002). HW83 = Harrison and Watson (1983). Boehnke13 = Boehnke et al. (2013). RH07 = Rubatto and Hermann (2007). DH82 = Dickinson and Hess (1982). The red solid line in all panels is a fit to our data at different pressures and H_2O contents. The black solid line in (f) is a fit to all data. The cyan dashed line in (f) is the equation of Boehnke et al. (2013).

This is a preprint, the final version is subject to change, of the American Mineralogist (MSA)
Cite as Authors (Year) Title. American Mineralogist, in press.
(DOI will not work until issue is live.) DOI: http://dx.doi.org/10.2138/am-2016-5462

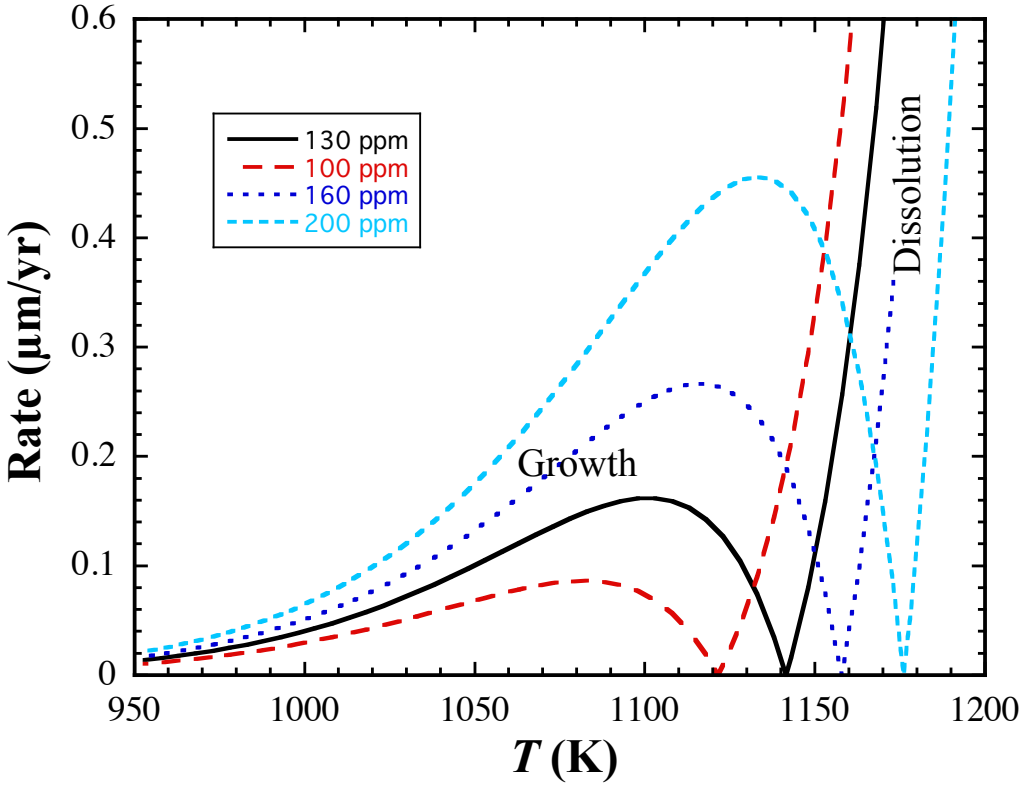

Fig. 10. Calculated convective zircon dissolution or growth rate as a function of temperature and Zr concentration in the melt. The melt composition is Rhy5 with 5.5 wt% H_2O. The radius of zircon is 30 μm. Surface tension effect is ignored. The pressure is 0.5 GPa. The minimum (where rate = 0) on each curve is at the temperature at which zircon is in equilibrium with the melt. Above this temperature, zircon dissolves; below this temperature, zircon grows.

This is a preprint, the final version is subject to change, of the American Mineralogist (MSA)
Cite as Authors (Year) Title. American Mineralogist, in press.
(DOI will not work until issue is live.) DOI: http://dx.doi.org/10.2138/am-2016-5462

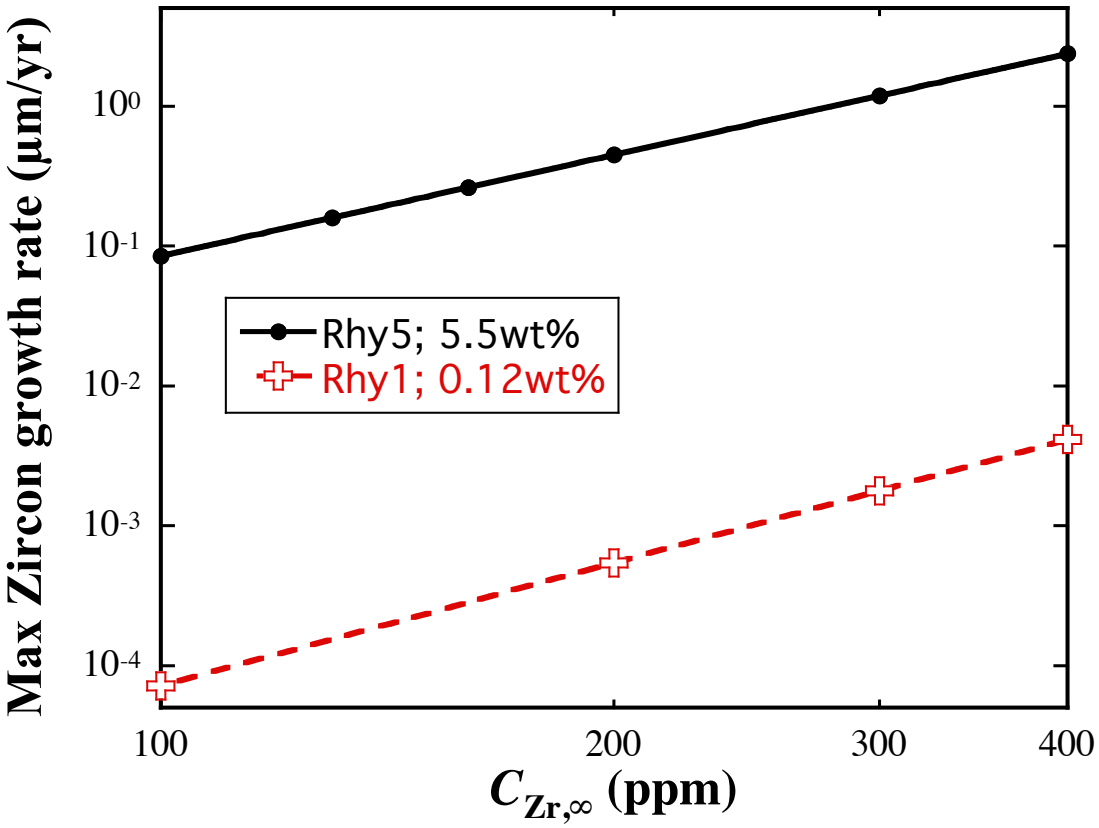

Fig. 11. Calculated maximum zircon growth rate in hydrous melt Rhy5 (with 5.5 wt% H_2O) and in dry melt Rhy1 (with 0.12 wt% H_2O). The calculation is carried out for a zircon crystal of 30 μm radius for several Zr concentrations. Convective zircon growth rate depends weakly on the crystal size. The line is fit by a power function, which fits the data almost perfectly, with $r^2 \geq 0.999999$.